

Effect of PEGylation on Physical and Biological Behavior of Temperature-Responsive Nanogels

Vahid Forooqi Motlaq



Thesis submitted for the degree of
Master of Science in Chemistry
60 credits

Department of Chemistry

Faculty of Mathematics and Natural Sciences

UNIVERSITY OF OSLO

June 10th, 2017

© Vahid Forooqi Motlaq – Department of Chemistry, Faculty of Mathematics and Natural Sciences, University of Oslo

2017

Effect of PEGylation on Physical and Biological Behavior of Temperature-Responsive Nanogels

Vahid Forooqi Motlaq

<http://www.duo.uio.no/>

The University Print Centre, University of Oslo

Abstract

The demand for thermo-responsive nanogels as drug delivery vehicles is high. Nanogels with potential application in the field of biomedicine should be stable against aggregation, and should not provoke immune response in the body. In the current study poly (*N*-isopropyl acrylamide)-co-(methacrylic acid) (PNIPAAm) nanogels were synthesized using *N,N'*-Bis (acryloyl)cystamine (BAC) as cross-linker. Polyethylene (PEG) with different lengths and surface concentrations were anchored to the surface of the nanogels in order to prevent them from aggregation. In addition hydrophilicity of the anchored PEG layer makes the surface of the nanogels more biocompatible. PEG with molecular weight of 2000, 5000, and 13000 were used. PEG 2000 and 5000 were used at 0.05, 0.5 and 1 mole % concentrations, and PEG 13000 was used at 0.05 mole % concentration.

Successful synthesis of nanogels was confirmed by nuclear magnetic resonance (NMR). The zeta potential measurements were conducted on nanogels in deionized water and in the presence of SDS to study the electrical surface charge at various temperatures. Turbidimetry measurements showed that as PEG length and/or surface concentration increased, cloud point (CP) shifted towards the higher temperatures suggesting a more stable system. Dynamic light scattering (DLS) results indicated that hydrodynamic radii (R_h) of nanogels grew with temperature except for the nanogels with the highest PEG length. The results from small angle neutron scattering (SANS) experiments indicated that the core of all nanogels was almost at the same size which showed that synthesis process proceeded meticulously. Furthermore, the combination of SANS and DLS results suggested a core-shell structure for the synthesized nanogels.

Cytotoxicity was measured with a colorimetric assay for different nanogels using MDA-MB-231 breast cancer cells after 24 hours. The results indicated that nanogels with PEG-5000 and 0.5 mole % concentration had the highest cell viability. Uptake of nanogels by human THP-1 macrophage was investigated after six hours and nanogels with PEG-5000 and 0.5 mole % concentration provoked the least immune response.

Acknowledgment

I would like to express my special thanks of gratitude to my main supervisor, Professor Bo Nyström, for his patience, motivation, enthusiasm and immense knowledge. His advice and insight was valuable to me in the time of research and writing of this thesis. I also would like to express my gratitude to my co-supervisor at cancer research institute located at Norwegian Radium Hospital, Dr. Shahla Bagherifam for her insight and performing biological experiments. I am also thankful to Dr. Kenneth Dahl Knudsen at the Institute for Energy Technology (IFE) for his advice and help with conducting and analyzing small angle neutron scattering experiments.

My special thanks to Masoud Kaboli and Jonas Andre Olsen for allowing me to use their laboratory accessories. I sincerely appreciate Julie Nitsche Kvalvik for her constructive comments on my thesis. I wish to express my warm and sincere thanks to Professor Frode Rise who taught me advance nuclear magnetic resonance techniques and gave me the opportunity to participate and present my work as a poster in national MR meeting (2016) in Bergen.

During my two years of studies I made some fantastic friends Sara Bekhradnia, Darya Zeini, Elahe Jafari. Thanks for helping me with everything, for the long days we were working together, and for all the fun we have had in the last two years.

Finally, I must express my very profound gratitude to the people closest to me. I would like to thank my parents and my sister Venus, for providing me with unfailing support and continuous encouragement throughout my years of study. Last but not least, my gratitude goes to my beloved wife. Leva thank you for all you have done for me, especially through the process of researching and writing this thesis. This accomplishment would not have been possible without you.

Vahid Forooqi Motlaq

Oslo, June 10st, 2017

Abbreviations

AF4 Asymmetric flow field-flow fractionation

BAC *N,N'*-Bis (acryloyl)cystamine

DCM Dichloromethane

DDL Diffuse double layer

DDS Drug delivery systems

DLS Dynamic light scattering

DLVO Derjaguin–Landau–Verwey–Overbeek

EDL Electrical double layer

LCST Lower critical solution temperature

MAA Methacrylic acid

NIPAM *N*-isopropyl acryl amide

NMR Nuclear magnetic resonance

PEG Polyethylene glycol

PEGMA Polyethylene glycol methyl ether methacrylate

PNIPAAM Poly *N*-isopropyl acryl amide

SANS Small angle neutron scattering

SDS Sodium dodecyl sulfate

SFEP Surfactant-free emulsion polymerization

SFPP Surfactant-free precipitation polymerization

SLD Scattering length density

Symbols

$g^1(q, t)$ First order electric field autocorrelation function

ΔG^{att} Gibbs free energy of attraction

ΔG^{rep} Gibbs free energy of repulsion

A_H Hamaker constant

A_f Amplitude for fast relaxation time

A_s Amplitude for slow relaxation time

I_0 Incident laser light intensity

I_t Transmitted intensity

R_h Hydrodynamic radius

U_e Electrophoretic mobility

$g^2(q, t)$ Intensity auto-correlation function

β_f Stretch exponent of fast mode

β_s Stretch exponent of fast mode

ε_{min} Depth of potential well

τ Turbidity

τ_f Fast relaxation time

τ_s Slow relaxation time

ΔG Gibbs free energy

h Plank's constant

D Mutual diffusion coefficient

E Potential gradient

$P(q)$ Form factor

$S(q)$ Structure factor

T Temperature (kelvin)

d Distance

$f(Ka)$ Henry's function

k Boltzmann constant

n Refractive index

q Wave vector

ν Characteristic frequency for the first ionization potential

α Polarizability

ε Dielectric constant

ζ Zeta potential

η Viscosity

Table of Content

Abstract	IV
Acknowledgment	VI
Abbreviations	VII
Symbols	VIII
1 Introduction	1
1.1 PEGylation	2
1.2 Drug delivery systems	2
1.3 Nanoparticles for drug delivery systems	3
1.3.1 Micelles	4
1.3.2 Dendrimers	4
1.3.3 Polymerosomes	5
1.3.4 Microgels	6
1.4 Colloid stability	7
1.4.1 Attractive forces	8
1.4.2 Electrostatic stabilization	9
1.4.3 Steric repulsion	10
1.5 Aggregation	12
1.5.1 Effect of aggregation on biological response	13
1.6 Microgels preparation	13
1.6.1 Homogeneous approach	15
1.6.2 Heterogeneous polymerization (emulsification)	16
1.7 Thermo-responsive nanogels	16
1.8 The Hofmeister effect on polymers	17
1.9 Definition of thesis	19
2 Backgrounds of methods	20
2.1 Dynamic light scattering (DLS)	20
2.2 Zeta potential	22
2.3 Turbidimetry	23
2.4 Small angle neutron scattering (SANS)	24
2.5 Nuclear magnetic resonance (NMR)	26
3 Experimental	28

3.1	Synthesis-----	28
3.1.1	Monomers purification -----	28
3.1.2	Synthesis of nanogels -----	31
3.2	Physical chemistry methods-----	34
3.2.1	Dynamic light scattering (DLS)-----	34
3.2.2	Small angle neutron scattering (SANS) -----	35
3.2.3	Turbidimetry-----	35
3.2.4	Zeta potential -----	35
3.2.5	¹ H NMR -----	36
3.3	Biological experiments-----	36
3.3.1	<i>In vitro</i> cytotoxicity -----	36
3.3.2	Macrophage uptake -----	37
4	Results -----	38
4.1	Synthesis of PEGylated poly (N-Isopropylacrylamide-co-methacrylic acid) -----	38
4.2	Zeta potentials -----	40
4.3	Turbidimetry-----	42
4.4	Dynamic light scattering (DLS)-----	47
4.5	Small angle neutron scattering (SANS) -----	53
4.6	<i>In vitro</i> cytotoxicity -----	58
4.7	Macrophage uptake -----	61
4.8	Complementary discussion -----	63
5	Conclusion -----	65
5.1	Future work-----	66
	Bibliography -----	67
	Appendix-----	74
	Appendix I: NMR results -----	74
	Appendix II: Turbidity measurements-----	78
	Appendix III: Hydrodynamic radii for all samples in water and 2 mM SDS solution -----	79
	Appendix IV: Asymmetric Flow Field–Flow Fractionation (AF4) measurements -----	80

1 Introduction

The use of polymeric nanocarriers for drug delivery applications has opened new opportunities for targeting specific cells in the body such as cancerous cell. Nanocarriers are submicron-sized particles that can deliver drugs, as well as, macromolecules such as protein, peptide or genes to site of interest [1]. However, a major obstacle facing the development of new carries for drug delivery is the rapid clearance of nanocarriers from the blood stream by the cells of the liver and spleen macrophages [2]. Macrophages are important cells in our immune system that have been developed to protect our body from invasion by foreign objects [3]. It has been shown that nanocarrier properties such as size, surface charge and surface hydrophilicity are important factors that determine the biological response after entering the body. It has been generally accepted, that hydrophobic nanocarriers are cleared from the blood stream by macrophages more rapidly than nanocarriers with hydrophilic surfaces [4, 5].

To reduce macrophage uptake of nanocarriers surface modification techniques have evolved. Surface modification of nanocarriers can provide a longer circulation time in the blood stream [2]. Poly ethylene glycol (PEG) has shown to be effective for surface modification of nanocarriers due to its hydrophilicity, electrical neutrality and chain flexibility which minimizes the interaction of nanocarriers with biological components in the body [6].

The aggregation¹ of nanocarriers is another challenge facing drug delivery systems. Physiochemical properties of aggregated particles are generally different from individual particles. This results in different biological responses. From the toxicological perspective, particles' size, shape, solubility, and surface area are important parameters which can change the cytotoxicity profile. It has been shown that cell uptake, cytotoxicity and bio distribution are factors that can be altered by the aggregation process [7, 8].

This thesis seeks to find optimal PEG length and PEG surface concentration to protect nanocarriers from aggregation and being uptaken by macrophages. First, different nanocarrier systems for drug delivery are introduced; especial focus will be on nanogels which are the main

¹ Aggregation will be discussed in more detail later in this chapter.

nanocarrier studied in this thesis. Next, theories behind stabilization of colloidal systems are discussed in more details.

Thermo-responsive nanogels were extensively studied in this group. The studied nanogels were stabilized by electrostatic repulsion and adding surfactants. This study aims to use steric repulsion of PEG chains to stabilize nanogel systems and prevent aggregation. Furthermore, biological experiments are performed to find optimal PEG length and PEG surface concentration to avoid toxicity and immune response.

1.1 PEGylation

Modifying the surface of the particle with PEG (PEGylation) was introduced for the first time by Davies and Abuchowsky in 1977 [9, 10]. PEG is a bio-inert, FDA approved polymer which consists of ethylene oxide repeating units. PEG chains are available at different configurations, including linear or branch structures, and in different molecular weights [11]. The chain length, shape, and density of PEG on particle surface are important parameters affecting nanoparticles surface hydrophilicity and interaction with proteins. The attachment of PEG chains to different nano-structures (e.g. nanoparticles, proteins and peptides) is referred to as PEGylation [12].

PEGylation has shown promise as a method to improve the colloidal stability and *in vivo* performance of various nanocarriers [1]. The absorption of blood plasma protein on the surface of nanoparticles determines recognition by macrophages, a delayed plasma proteins absorption reduces macrophage uptake of nanocarriers (prolong circulation time). The relative long blood circulation of PEG surface modified nanoparticles is hypothesized to be related to a steric barrier provided by the attached PEG [13]. PEG molecules presumably form a dynamic molecular “cloud” over the particle surface, therefore, can arrest both protein absorption and aggregation [14]. First a brief introduction about drug delivery systems (DDS) and different nanocarriers used in DDS are disputed.

1.2 Drug delivery systems

Drug delivery systems have provided great opportunity in the field of medicine especially cancer therapy. These systems can be developed to minimize drug degradation and loss, reduce

side effects, and to increase the fraction of therapeutic agents in a specific part of body by encapsulating various therapeutic agents especially hydrophobic drugs. Administration of hydrophobic drugs is more difficult as they may precipitate in aqueous media [15].

In conventional chemotherapy drugs are administrated intravenously. The major drawback of this method is that a very small portion of the drug reaches the tumor after injection and most of the therapeutic agents will be rapidly cleared from blood circulation. The aim of DDS in cancer therapy is to enhance drug concentration at the target cells while reducing the effective levels for normal cells. Consequently, the efficiency of drugs increases and their side effects decrease [16].

1.3 Nanoparticles for drug delivery systems

During the past decades, different types of nanocarriers have been developed for DDS. Nanocarriers are submicron-sized particles that can deliver drugs, as well as, macromolecules such as protein, peptide or genes to site of interest. Nanocarriers can encapsulate therapeutic agents and provide targeted delivery and slow release, which increases their efficiency and protect drugs from degradation by enzymes in the body. Polymeric nanocarriers are the most studied type of nanocarriers for DDS [1]. Four major polymeric nanocarriers have been studied so far for DDS namely, micelles, dendrimers, polymerosomes and microgels/nanogels [17, 18]. Figure 1-1 illustrates examples of nanocarriers commonly used as drug delivery systems.

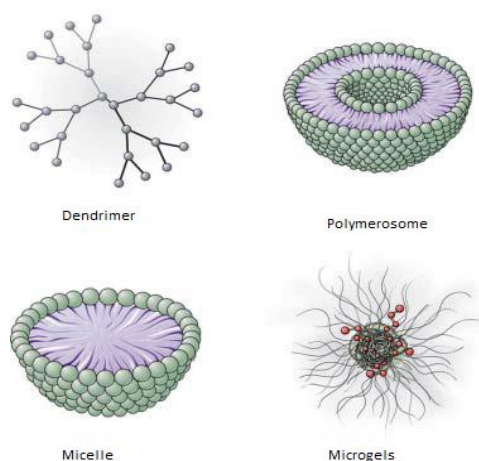


Figure 1-1: General architecture of nanoparticles commonly used as drug delivery carriers. Figure adopted from reference [1].

1.3.1 Micelles

Amphiphilic block copolymers are a group of macromolecules composed of hydrophobic and hydrophilic blocks. The difference in solubility between the blocks in aqueous medium is a characteristic property of amphiphilic block copolymers. Polymeric micelles can be formed by self-assembling of unimers² from amphiphilic copolymers above a critical micelle concentration (CMC) in a specific solvent. Different classes of materials can self-associate to form micelles, e.g. amphiphilic block copolymers are one major group with this potential [19].

Amphiphilic copolymers tend to form core-shell architectures in aqueous medium; the core is composed of hydrophobic segments, whereas the shell is formed by hydrophilic chains. This phenomenon happens because the amphiphilic block copolymer rearranges itself in such a way that the hydrophobic chains avoid water contact. Micelles demonstrate a number of interesting properties, including ease of production, nanosize (generally ≤ 100 nm) and narrow size distribution, core functionalities, easy manipulation of core or shells and free space in the core. All of these make them good candidates for DDS, particularly for hydrophobic chemotherapeutics compounds. Micelles can solubilize hydrophobic pharmaceutical agents in the core, while the hydrophilic shell provides stability. Although micelles exhibit good colloidal stability, they are not considered as solid particles [19-21].

1.3.2 Dendrimers

The word “dendrimer” comes from Greek word, “dendra”, which means “tree”, and “meros”, which means “part of”. They are a class of synthetic organic polymers with a structure similar to a tree. These macromolecules constitute one core and layers of repeating unit which are diverged from the central core. The layers branch off from the core to the periphery, and each layer is identified as a generation (G1, G2, etc.). They have a number of unique features, including a monodisperse size distribution, spherical structure, as well as high density of surface functionality which make dendrimers suitable for biomedical applications [22, 23].

² Unimers are the solo subunit of a micelle.

The first report on dendrimers was published by Tomalia's group in 1985 [24]. Since then they have attracted a great deal of interest due to their unique properties. These materials have a lower viscosity compared to linear polymers and their solubility is controlled by their functional group on the surface. Dendrimers have a well-defined architecture and benefit from high density of functional terminal groups on the surface, which provides many positions for binding with drugs and receptors. They can encapsulate drug molecules via covalent and non-covalent (electrostatic, hydrophobic, and hydrogen-bond) bonds. Their controllable size and globular shape enable them to mimic proteins without provoking immune response. All these properties make them suitable for various applications such as drug delivery, cancer therapy and gene delivery [22, 23].

1.3.3 Polymerosomes

Polymerosomes are "polymeric vesicles" of amphiphilic block copolymers in nanometer dimensions that are formed by a self-assembly process in dilute aqueous media. Vesicles are similar to micelles, but they consist of bilayer membrane (see Figure 1-1). A vesicle's bilayer is composed of two layers of hydrophobic segments, and unlike micelles the core of vesicle is comprised of an aqueous phase [25].

Polymerosomes have a hollow-spherical structure with an approximate size of 50 nm to 1 μ m, depending on the nature of block copolymer and the preparation method. Polymerosomes can mimic liposomes that are spherical lipid vesicles inside cells. While the immune response induced by polymerosomes is at the same level as that of liposomes, they display a remarkably higher mechanical stability, since the membrane of polymerosomes may be up to ten times thicker than those of forming liposomes. Polymerosomes can encapsulate the therapeutic drug inside and/or inserted within membrane; as a result both hydrophobic and hydrophilic drugs can be carried by them. On the other hand, polymerosomes can be functionalized to specific stimuli responsiveness as well as for different targeting approaches [26-28].

The important component of polymerosomes is their membrane which determines the permeability of polymerosomes to both hydrophobic and hydrophilic compounds. Membrane permeability can be tailored by changing the functionality or length of the

hydrophobic/hydrophilic block. Membrane flexibility is crucial for the diffusion of different compounds into polymerosomes which will be reduced as the block copolymer molecular weight increases[26, 27].

1.3.4 Microgels

Microgels/nanogels,³ topic of this study, are three-dimensional non-linked aggregated polymer networks of finite size that are formed via intramolecular cross-links. On the other hand, macrogels (hydrogels) are 3D-networks of polymer chains that are connected via intermolecular cross-links. The size of macrogels depends on the size of its container. In both macro- and micro- gels, the polymer chains are kept in the structure by physical or chemical bonds. Although there is no universal description for microgels, the most common one is: “a polymer colloid particle which swells in a good solvent”. A solvent is a “good solvent” if the mixture is homogeneously dispersed, and interactions between a polymer chains and adjacent solvent molecules are energetically favorable, causing polymer coils to expand [29, 30].

The first microgels were synthesized by Husemann and Staudinger in 1935 [31] and the term “microgel” was introduced by Manson in 1949 [32]. In contrast to a responsive polymer solution that phase separates in response to pH or temperature and precipitates, responsive microgels or macrogels will shrink and expel the solvent. This transformation is referred to as volume phase transition and the temperature is called volume phase transition temperature (VPPT) [33].

Microgels have attracted great interest as model colloids and for their potential applications in drug delivery. The interior network of microgels can be functionalized to allow the incorporation of either hydrophobic or hydrophilic drugs. It has been proved that microgels can be designed to respond to external stimuli such as magnetic field, light, temperature, and pH; the release drug profile can be modulated by these external stimuli. As a result, microgels could uptake drugs in the swollen form and release it in response to external triggers. These features make responsive microgels a good nanocarrier for biomedical applications [18, 34].

³ The term microgels and nanogels have been used in literature interchangeably; however nanogel term is more common for particles that are less 100 nm.

The most prominent and well-studied temperature responsive polymer is poly N-isopropyl acryl amide (PNIPAAm) with VPPT of around 32 °C. The phase transition of PNIPAAm has been immensely studied throughout the years. It has been shown that VPPT could be modified by changing molecular weight, topology, polymer concentration, and functionalizing with co-monomers (e.g. acrylic acid, methacrylic acid). Microgels have some unique characteristics; such as high colloidal stability, ease of preparation, a tunable size and tailorable structure. In swollen form, they contain high water percentage and can change conformation in response to pH, temperature, ionic strength, UV light, magnetic field, ultrasound, enzymes, etc. The “stimuli responsive” microgels exhibit exceptional properties which stem from the particular combination of their colloidal nature with their internal network structure. These stimuli-responsive properties are an area of increasing interest as “smart materials” since they respond to their environments [33, 35, 36].

1.4 Colloid stability

The term colloid⁴ (glue-like) was first proposed by Thomas Graham. Colloids are an intermediate class of materials going between bulk and molecularly dispersed systems. They consist of a dispersion medium (solid, liquid or gas) and a dispersed phase or phases (solid, liquid or gas) that are dispersed in uniformly. Colloids usually are in the range 1-1000 nm, nanocarriers used in DDS mostly lying in this range [37].

During the formation of colloids, the surface-to-volume ratio increases as the size of colloids reduces. This excess surface free energy contributes to the special properties of the colloids. Surface-to-volume ratio of colloids is high and their special properties originate from molecules in the interfacial areas. This high surface area makes the thermodynamic properties of the colloid different from its bulk state. From what has been discussed, it is evident that colloids are in a higher state of free energy compared to their bulk form. So, there should be some strong energy barriers preventing them from forming aggregates. Colloid particles are subject to different forces that can be categorized as attractive and repulsive forces. The attractive force is Van der Waals interactions, while electrostatic repulsion and steric stabilization are two

⁴ Although the term colloid is widely accepted, the etymology is now largely irrelevant.

mechanisms that prevent colloid particles from aggregating. The result from these intermolecular and surface forces determines the colloidal stability [8, 37].

1.4.1 Attractive forces

For investigating attractive forces between a pair of colloid particles, first, it would be useful to look in to origin of these forces for a pair of non-polar molecules. The classical work of Van der Waals showed the interaction between a pair of non-polar molecules caused by correlations in the fluctuating dipoles of nearby molecules. These forces rise in magnitude as two adjacent molecules approach one another. The equation (1-1) shows that these forces are proportional to the inverse of sixth power of distance.

$$\Delta G^{att} = -\frac{3/4h\nu\alpha^2}{d^6} \quad (1-1)$$

where α is the polarizability of atoms or molecules, h is Planck's constant, ν is characteristic frequency for the first ionization potential and d is the distance of atoms.

The attractive forces increase and, consequently, free energy becomes negative as the atoms come close, but as they approach, their electron clouds start to interact. At a very close distance this gives rise to repulsive forces and sharp increases in free energy. The repulsive forces can be expressed by the equation below (Born repulsion):

$$\Delta G^{rep} = \frac{B'}{d^{12}} \quad (1-2)$$

where B' is constant. The total potential energy of interaction between the pair of atoms (or molecules) can be described by the Lennard-Jones potential:

$$\Delta G = 4\varepsilon_{min} \left[\left(\frac{r_0}{d} \right)^{12} - \left(\frac{r_0}{d} \right)^6 \right] \quad (1-3)$$

where ε_{min} is the depth of potential well and r_0 is the distance at which the potential is zero. For two particles, the attractive forces can be described as the summation of all molecules in one particle that interact with each molecule in another particle, and repulsive forces can be neglected (due to the 12th power). For two particles at distance d apart and with radius R , when particles in close proximity ($D \ll R$) Van der Waals interactions can be calculated by the Hamaker relation:

$$W^{att} = \frac{A_H R}{12d} \quad (1-4)$$

where A_H is the Hamaker constant and its value is in order ($10^{-19} - 10^{-21}$ J) [37].

The interactions that keep the two particles apart (repulsive forces) electrostatic and steric stabilization, will be discussed in the next part.

1.4.2 Electrostatic stabilization

In an aqueous medium, the surface of colloids may become electrically charged by various mechanisms (e.g. ionization of surface groups, adsorption of charged molecules or ions to the particle surface), and the charge is distributed over the surface. In an ionic medium, charged particles have a layer of counter-ions strongly attached to their surface. This layer of firmly bound counter-ions is referred to as a "Stern layer". A second layer, consisting of loosely associated ions and counter-ions forms around the Stern layer. This layer spreads out in the medium because of the thermal motion, developing a "diffuse double layer" (DDL). In colloid science, this ionic atmosphere (consisting of Stern layer and DDL) is described as the electrical double layer (EDL). There is an excess of oppositely charged ions (counter-ions) in the EDL and the colloid charge is balanced by the total charge in the EDL (see Figure 1-2). The potential of EDL

declines exponentially with distance from the surface [38, 39].

The concept of the EDL was first proposed by Helmholtz in the 1850s. Further investigations led to a more sophisticated and better understanding of the EDL. Repulsion of two particles in a medium by this theory can be described as follows: when two charged particles with the same charge come close in space, the two EDL overlap, and start to “feel” each other’s presence. This interaction increases steadily as they move toward one another. At a closer distance the Stern layer of particles with the same sign interact and repel one another. The repulsive forces reduce by the presence of ions in the medium [37].

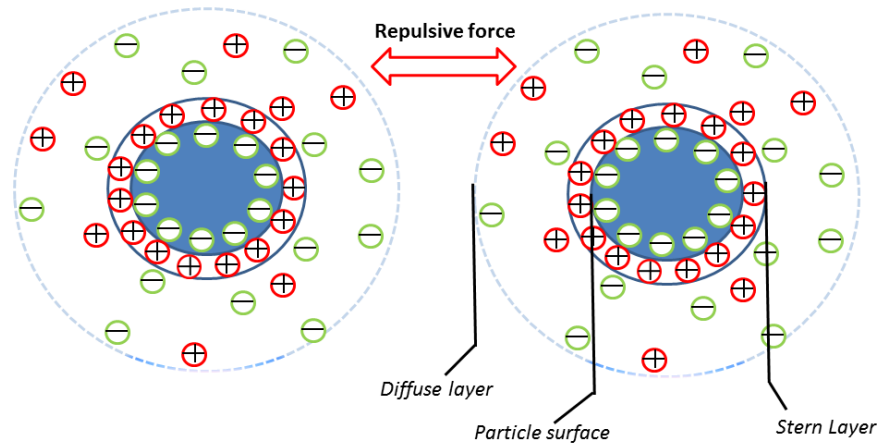


Figure 1-2: Schematic illustration of electrical double layer for two particles, and the resultant repulsive force.

1.4.3 Steric repulsion

It has been known from Faraday’s classic work on colloids that polymers can create a shell around the particles, which can lead to a steric stabilization of colloidal dispersion by affecting Van der Waals attractive forces. In addition, the adsorbed layer can cause an osmotic repulsion force between colloid particles [37].

When the particles are completely covered with a polymer layer, their radius will increase, if this layer is hard, the increase in particle radius prevents particles from coming closer than

" $R+\delta$ " (where δ is thickness of polymeric layer and " R " is particles radius). This increases the distance between two particles which reduce the attractive forces. If the coating layer does not behave like a hard surface (most of polymer coatings are in this category), it can prevent forming aggregates by elastic recoil effect upon collision between two particles. To prevent aggregation, the coating layer should have properties close to the medium rather than the particle (i.e. for aqueous medium the coating layer ought to be hydrophilic) [37].

The polymer layer around colloid particles can usually be seen as hairy chains extended out into the medium. Upon collision, two particles come close in space and the polymer chains from two particles overlap, and the local density of polymer chains between two particles increases. This increase in local polymer chains produces an osmotic pressure between two particles. As a result, the solvent will diffuse into the area between the particles and drive them apart (see Figure 1-3) [8, 37].

As the polymer chains of the two particles link together, number of positions the two particles can adopt reduces. Consequently, the entropy reduces and the Gibbs free energy increases. This increase in the free energy contributes to the intermolecular potential is called entropic repulsion [8, 37].

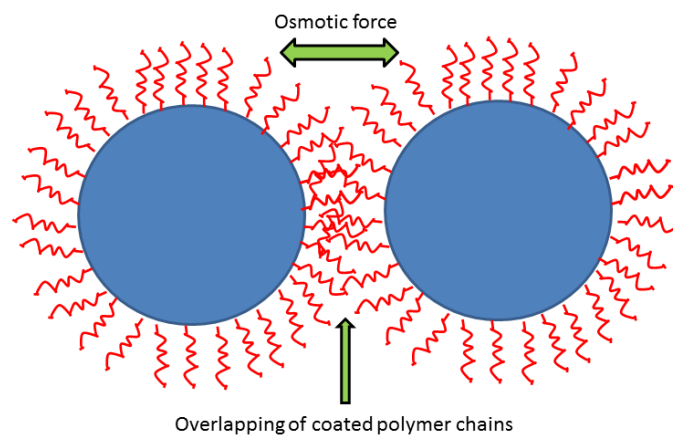


Figure 1-3: Schematic illustration of steric repulsion mechanism between two particles with polymeric coating.

1.5 Aggregation

Aggregation can be described as a process in which colloid particles come together to form a bigger particle. The first step of aggregation is called flocculation and occurs spontaneously. Flocs have an open structure while aggregates are denser and if they become big enough, they will ultimately sediment. In the absence of a high enough energy barrier, colloid particles tend to lower the total free energy by forming aggregates. This process can be reversible or irreversible. Stability of colloids comes from the balance between attractive and repulsive forces, net repulsive forces which are sufficiently high can prevent aggregation [37].

Derjaguin–Landau–Verwey–Overbeek (DLVO) theory was a theoretical approach to investigate the state of colloid [40]. The DLVO theory considers Van der Waals attractive forces and repulsive potential raised by the EDL to predict the stability of a colloidal system. Figure 1-4 shows the resulting total-interaction potential for a system with aggregation barrier. The attractive forces can be calculated from equation (1-4) [40]. In most situations, A_H is positive and indicates that Van der Waals forces between two particles are attractive. According to the original DLVO theory, the charge is uniformly distributed on the surface of particles and higher surface charge will result in a higher colloid stability. Two important parameters which affect system stability are the electrolyte ion type and concentration. While Van der Waals interaction is comparatively independent of the ion concentration, surface potential decreases exponentially with increasing the ion concentration. This means that a higher ion concentration the aggregation process is more favorable. Furthermore, DLVO theory discloses that the colloid stability increases with increasing particles' size and bigger particles are more stable than smaller ones [8, 39].

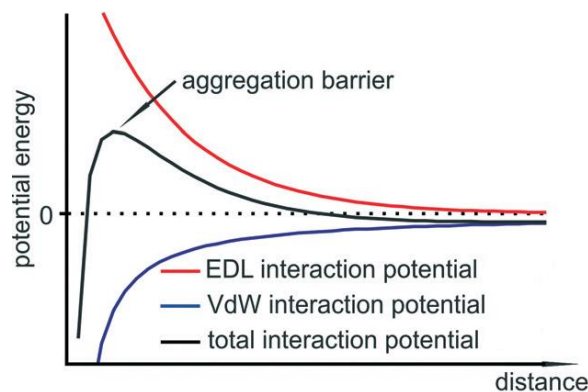


Figure 1-4: Total-interaction potential resulting from Van der Waals (VdW) attractive and electric double layer repulsive (EDL) forces. Figure adopted from reference [39].

1.5.1 Effect of aggregation on biological response

Aggregation process is usually described as an irreversible inter-particle adherence by which large and irregularly shaped associations are formed. Aggregation can lead to a change in several biological responses, including cellular uptake and toxicity of particles. This can cause different problems such as misrepresentative result and disrupt experimental reproducibility. Aggregation of intravenously administered particles can lead to rapid clearance from the blood stream, limiting the fraction of nanoparticles which reach their therapeutic target. Moreover, in vivo experiments, big aggregates could lead to capillary blockage and subsequent morbidity [8].

Most aggregates show a random shape and disordered structure. Aggregates have versatile packing densities, so they will not just act like a large single particle with an equally large hydrodynamic radius. In comparison to dispersed particles, aggregated particles exhibit a lower diffusion rate and different sedimentation velocities. The specific surface area is one another feature that changes by aggregation. A lower surface area causes a smaller ratio of particle atoms or molecules to be exposed on the surface. Aggregated particles can trigger different biological responses than a single particle. Therefore, it is necessary to study aggregation processes and mechanisms for biological applications [7, 8, 41].

1.6 Microgels preparation

There are three different starting points for microgels synthesis:

1) From macrogels: Microgels can be prepared by mechanically grinding a macrogel; however, there are a few successful reports in the literature [42]. Most of the efforts in this respect have resulted in randomly shaped and irregularly structured microgels [43].

2) From polymer: Microgels can be synthesized from prepared polymer solutions. It is possible to cross-link oligomeric precursor chains by physical or chemical bindings to form microgels. In the case of physical binding, oppositely charged interaction or hydrophobic-hydrophilic interaction can be the binding agent. On the other hand, for the chemical binding, normal cross-linkers can be used to connect polymer chains, or two sets of oligomers can be

functionalized with different moieties which react with each other upon mixing (Figure 1-5) [33, 44].

3) From monomer: This is the most common approach to prepare microgels and has been studied more than any other methods. Many vinyl monomers and some bi-functional monomers as cross-linkers can be used in this method. It will be discussed in following section [33].

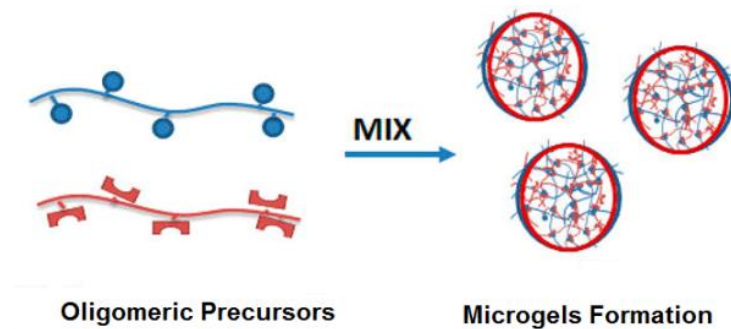


Figure 1-5: Synthesis of microgels from oligomeric precursors. Figure adopted from reference [44].

There are two main approaches for microgels preparation, (1) homogeneous (or nearly so) phase polymerization and (2) heterogeneous phase polymerization. In homogeneous phase polymerization, while the free radical initiator is soluble in the polymerization solution, the formed polymer is insoluble over the polymerization condition. When the monomers are soluble or nearly soluble in the polymerization condition, macrogels instead of microgels will form. In heterogeneous phase polymerization, monomer is insoluble in a continuous phase, and a solution of “pregel” droplets, consisting of a monomer or monomers, is suspended in a continuous phase to form an emulsion. The polymerization reaction happens inside pregel droplets [18, 33].

1.6.1 Homogeneous approach

Two common methods for the homogeneous microgels preparation are emulsion polymerization and surfactant free emulsion polymerization. Surfactant-free emulsion polymerization (SFEP) and surfactant-free precipitation polymerization (SFPP) are subdivisions of surfactant-free preparation. The mechanism for surfactant-free techniques can be described as the following: the initiator decomposes (e.g. thermal or light decomposition) to form the free radicals to initiate polymerization. When the chain length of the formed oligomers (low molecular weight polymer chains) surpasses the solubility of the solvent, they undergo limited aggregation, thus forming particle nuclei that are not colloidally stable (nucleation process). Further growth of the particle occurs by the coalescence of nuclei and adsorption of monomers or oligomers. As the particle grows, the charged chain ends accumulate on the surface of the particles, until the growing particles reach a certain point where they are colloidally stable. The presence of a cross-linker is important to prevent the dissolution of the formed particles. The term of "SFEP" is used in a case where droplets of monomers are present in the aqueous phase and serve as reservoir, but in the SFPP, monomers are water soluble, the formed polymers from both techniques (SFEP and SFPP) are insoluble over the polymerization condition (e.g. polymerization temperature). In the SFEP technique formed polymer chains are stabilized by initiators ions [33, 45, 46].

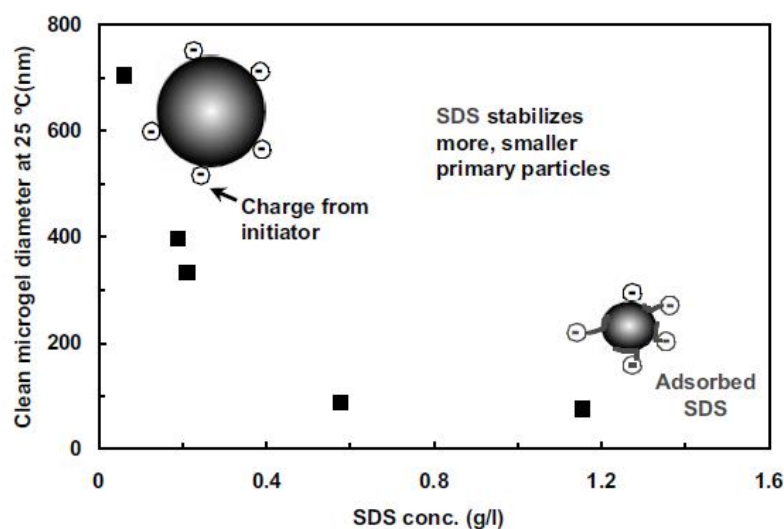


Figure 1-6: Effect of SDS concentration on PNIPAM microgel size. Figure adopted from reference [33].

It has been shown that adding surfactants during the microgel fabrication influences the nucleation and reduces the size of microgels (see Figure 1-6). Sodium dodecyl sulfate (SDS) is the most studied surfactant for microgels preparation. In the emulsion polymerization method, polymerization occurs inside the micelles. In this process, first, surfactant molecules form micelles and then monomers concentration increases inside the micelles through the adsorption of monomers. After that, water soluble initiator is added and diffused into monomers-swollen micelles. Subsequently, by the decomposition of the initiator (e.g. thermal, redox), free radicals are formed. The polymerization will continue by the diffusion of monomer into micelles which makes the rate of polymerization constant [18, 33, 47].

1.6.2 Heterogeneous polymerization (emulsification)

In heterogeneous phase polymerization, the solution of monomer or polymer is dispersed in the second medium to form emulsion droplets, and polymerization and crosslinking occurs inside each emulsion droplet, and they serve as “nanoreactors”. Microemulsion and miniemulsion are the two common methods in heterogeneous phase polymerization. Both methods can be realized as oil-in-water (O/W) or inverse water-in-oil (W/O) emulsions. The inverse microemulsion method for water swellable hydrogel nanoparticles has been largely studied. In this method, firstly, a pregel aqueous solution of monomers and cross-linkers is added to the continuous organic phase containing oil soluble surfactant. In the next step, microemulsion will form by stirring the mixture. The polymerization can be initiated either from inside the droplets or by adding free radical precursors to the continuous phase. In heterogeneous phase polymerization usually, the initiator is added to the oil phase and diffused into the droplets [18, 33].

1.7 Thermo-responsive nanogels

Smart polymers are able to respond to external stimuli such as pH, temperature, ionic strength, electric or magnetic field. These polymers gained attention especially in the field of drug delivery, tissue engineering, and bio-sensing. Among different stimuli, temperature is an easy external stimulus to apply and thermo-responsive polymers offer interesting properties for drug delivery systems [48].

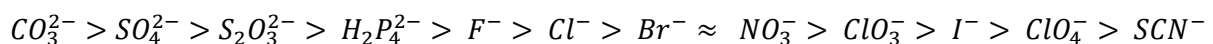
There are two main types of thermo-responsive polymers; the first group shows a lower critical solution temperature (LCST) and the second an upper critical solution temperature (UCST). The focus of this thesis is on PNIPAAm which is a thermo-responsive polymer with a LCST behavior [49].

LCST behavior was first documented by Heskings and Guillet for an aqueous solution of PNIPAAm [49]. Polymers with LCST behavior are soluble in water due to formation of hydrogen bonds with the surrounding water molecules, and restricted intra- and intermolecular hydrogen bonding between polymer molecules. The hydrogen bonding with water molecules is disrupted upon heating and intra- and intermolecular hydrogen bonding/hydrophobic associations control the solubility. This leads to a transition in solubility which provides interesting prospects in bio-medical field. If a polymer has a transition temperature between room and body temperature, drug molecules can be dissolved and trapped within a polymer network at room temperature and released when the system contracts due to a change in temperature in the body [50].

LCST can be adjusted by copolymerization with hydrophilic or hydrophobic co-monomers. Increasing hydrophilicity of polymers increases the ability of polymers to form hydrogen bonding which in turn leads to a higher transition temperature. While, increasing hydrophobic interactions by incorporating more hydrophobic groups in the polymer backbone lowers LCST by disrupting the structure of water molecules around the polymer [51].

1.8 The Hofmeister effect on polymers

In 1888 Franz Hofmeister proposed that the tendency of salts to precipitate certain proteins (salting-out), follows a specific order. This is an important effect in biology and chemistry, and salinity may influence different phenomena including protein stability, enzyme activity, macromolecule crystallization, as well as protein and polymer folding. This effect is more pronounced for anions than cations and the order of anions in Hofmeister series is:[52]



Salting-out refers to as a decrease in solubility of a nonelectrolyte with increasing the concentration of electrolyte. The opposite phenomenon is known as salting-in. The species on the left are consisting of small ions with high charge density and called kosmotropes whereas, the species on the right, large ions with small charge density, are referred to as chaotropes. Kosmotropes are considered “water making structure” with a thick hydration shell and chaotropes are considered “water breaking structure” with a thin hydration layer. The presence of kosmotrop anions in an aqueous solution of polymer leads to a higher surface tension, lower solubility of macromolecules, and salting-out effect (aggregation of molecules). For polymers in the presence of chaotrop ions, the effect is usually reduced surface tension and enhanced macromolecular solubility and salting-in effects [53].

1.9 Definition of thesis

The aim of this thesis is to investigate the effect of PEGylation on colloidal stability of nanogels with potential application in the field of drug delivery. This study contributes to three different fields: synthesis of nanogels, characterization of the synthesized nanogels and biologicals assays.

In order to study the effect of PEG length and PEG surface concentration on the stability of colloidal systems, eight different nanogels are synthesized in total. Emulsion polymerization is employed to fabricate PNIPAAm nanogels covered with a PEG layer at certain length and surface concentrations. Nuclear magnetic resonance technique is used to study the polymerization process.

The effect of PEG length and PEG surface concentration on colloidal stability is investigated through zeta potential, DLS, turbidimetry and SANS measurements. The effect of temperature on stability of the colloidal system with and without adding extra surface charge will also be studied.

To study the optimal PEG length and PEG surface concentration for biomedical applications, cytotoxicity of nanogels in MDA-MB-231 breast cancer cell line is measured with a colorimetric assay. To investigate the effect of PEGylation on suppressing the recognition of nanogels by the immune system, uptake of nanogels by THP-1 human macrophages is visualized by confocal microscopy.

2 Backgrounds of methods

In this section the background theories of the methods which used for characterization of the samples are discussed.

2.1 Dynamic light scattering (DLS)

DLS is a powerful technique to investigate time-dependent features of polymers and colloids in solutions. DLS gives the opportunity to explore the dynamic and structural features of the samples such as diffusion coefficient, hydrodynamic radius and size distribution of particles. In this method, the beam of laser passes through the solution and the random fluctuation in scattered light intensity is recorded by the detectors. This random fluctuation is due to the Brownian motion of macromolecules in the solution. It is possible to investigate the relaxation of concentration fluctuation at length scale of q^{-1} , through the registration of these time-dependent fluctuation [54].

$$q = \frac{4\pi n}{\lambda} \sin\left(\frac{\theta}{2}\right) \quad (2-1)$$

In equation (2-1), q is the wave vector, λ is the wavelength of incident light in vacuum, n is the refractive index of the medium and θ is the scattering angle. The q times R (e.g. R_g or R_h in a very dilute regime) defines whether the sample is probed on a local ($qR > 1$) or on global ($qR < 1$) length scale [55].

If the scattered field obeys Gaussian statistics, the experimentally measured intensity auto-correlation, $g^2(q, t)$, is related to the first-order electric field correlation function, $g^1(q, t)$, by the Siegert formula [56]:

$$g^2(q, t) = 1 + B |g^1(q, t)|^2 \quad (2-2)$$

where $B (\leq 1)$ is the instrumental parameter. The decay of the correlation function is described by a bimodal stretched exponential:

$$g^1(q, t) = A_f \exp \left[- \left(\frac{t}{\tau_{fe}} \right)^{\beta_f} \right] + A_s \exp \left[- \left(\frac{t}{\tau_{se}} \right)^{\beta_s} \right] \quad (2-3)$$

$$A_f + A_s = 1 \quad (2-4)$$

where parameters A_f and A_s are the amplitude of fast and the slow mode, consecutively, and τ_f and τ_s are the fast effective relaxation time and the slow effective relaxation time, respectively. Parameter $\beta (0 < \beta \leq 1)$ is the measure of the width of the distributions of relaxation times, and is related to the polydispersity of the system. The mean relaxation times can be calculated with the help of gamma function (Γ).

$$\tau_f = \frac{\tau_{fe}}{\beta_f} \Gamma \left(\frac{1}{\beta_f} \right) \quad (2-5)$$

$$\tau_s = \frac{\tau_{se}}{\beta_s} \Gamma \left(\frac{1}{\beta_s} \right) \quad (2-6)$$

If the relaxation times are q^2 dependent the system is diffusive and the times can be related to the mutual diffusion coefficient through the following equation:

$$\tau_f^{-1} = Dq^2 \quad (2-7)$$

The hydrodynamic radius of (R_h) can be determined by Stokes-Einstein relation:

$$R_h = \frac{kT}{6\pi\eta D} \quad (2-8)$$

where k is the Boltzmann constant, T is the temperature and η is the viscosity of the medium [57].

2.2 Zeta potential

Electrically charged colloid particles develop an electrical double layer (EDL) around them, which was discussed in 1.4.2. Charged colloid particles move under the influence of an external electric field (electrophoretic mobility). There is a hypothetical boundary plane within the diffuse layer which acts as an interface between the moving colloid particles and the ions that move along with them, and the ions left behind. The outer limit of this boundary layer is often called the slipping or shear plane. The slipping plane is located between the Stern layer and the DDL (see Figure 2-1) [58, 59].

Zeta potential is an effective electrostatic potential at the slipping or shear plane. Since the exact location of the slipping plane is hard to define, the zeta potential can be seen as an ambiguous measurement of potential difference between the medium and the stationary layer of ions around electrically charged particles. Zeta potential does not represent the Stern potential or electric surface potential in the double layer. However, it is usually the only valid method for investigation of the EDL [37, 59].

Zeta potential experiment determines the potential stability of colloidal systems, and the results can be interpreted as the degree of repulsion between adjacent particles. Colloid particles with zeta potential around ± 10 mV or lower are expected to be unstable; particles with a large negative or positive value ($\geq \pm 30$) are considered as stable colloid systems [60].

In a zeta potential measurement, the instrument measures the electrophoretic mobility of the particles by applying an electrical field across the sample. The electrophoretic mobility of a charged particle is the velocity by which charged particles move towards the opposite electrode. The zeta potential (ζ) can be obtained from Henry's equation:

$$U_e = \frac{2\varepsilon\zeta E}{3\eta} f(Ka) \quad (2-9)$$

where U_e is the electrophoretic mobility, E is the potential gradient (voltage applied/distance between electrodes), ε is the dielectric constant, η is the viscosity of the dispersion medium and $f(Ka)$ is Henry's function. The Smoluchowski approximation ($f(Ka) = 1.5$) was utilized [60].

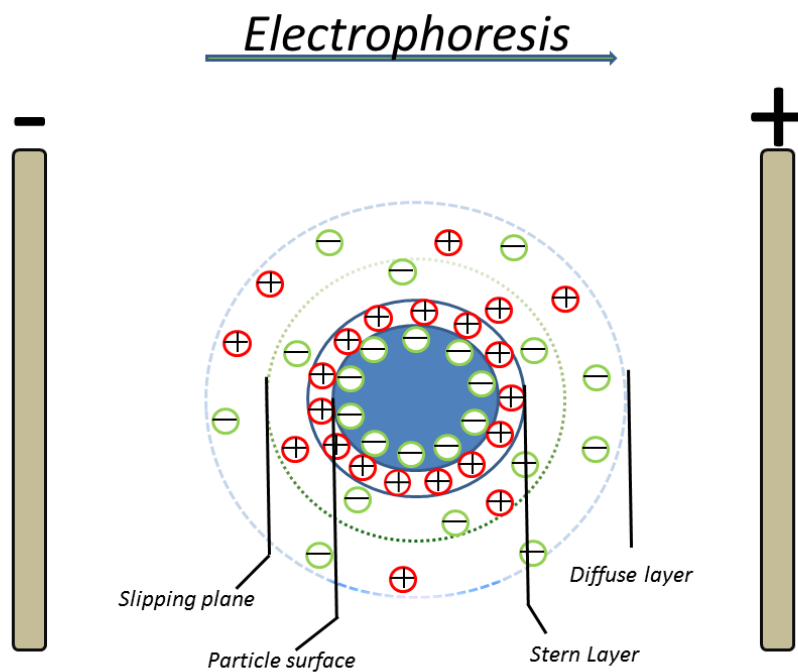


Figure 2-1: Schematic illustration of the position of slipping plane in EDL.

2.3 Turbidimetry

Turbidity is cloudiness or opaqueness of a solution caused by number of suspended single particles inside a solution. In this method, the haziness of solution is determined by measuring the intensity of a transmitted laser light as function of temperature. In turbidimetry, as the incident beam pass through a solution, particles or aggregates in the solution can absorb or

scatter the beam. Subsequently, the scattered beam will be registered by a detector, and the degree of attenuation of its intensity corresponds to the turbidity level of the solution. The number of particles, their size and the refractive index difference between suspended particles and medium, are parameters which can affect the turbidity. The turbidity (τ) can be expressed as following equation:

$$\tau = \left(-\frac{1}{L}\right) \ln\left(\frac{I_t}{I_0}\right) \quad (2-10)$$

where L is the length that laser beam passes through the samples, I_t is transmitted intensity and I_0 is incident laser light intensity [61].

2.4 Small angle neutron scattering (SANS)

Small angle neutron scattering (SANS) is a powerful and non-invasive technique to investigate size, shape and internal structure of various systems ranging from 1 to 70 nm. In a SANS measurement, a neutron beam is passes through a sample, and the scattered beam is recorded by the detectors. The scattered beam is the result of collisions between neutrons and the nuclei of the atoms in the sample. The scattered intensity depends on nuclei atomic mass number; therefore various isotopes of an element may cause different intensities. This scattering power of materials is described as their “neutron scattering-length density” parameter. The scattered intensity for H_2O and D_2O differ considerably from each other so that by mixing different ratios of them, a wide range of background intensities are accessible. In the case of core-shell particles, one can match the background intensity of the solution to either core or shell, making one invisible and enables us to investigate the other. Moreover, SANS technique can be employed to characterize the concentrated opaque samples that cannot be investigated by light scattering technique [62, 63].

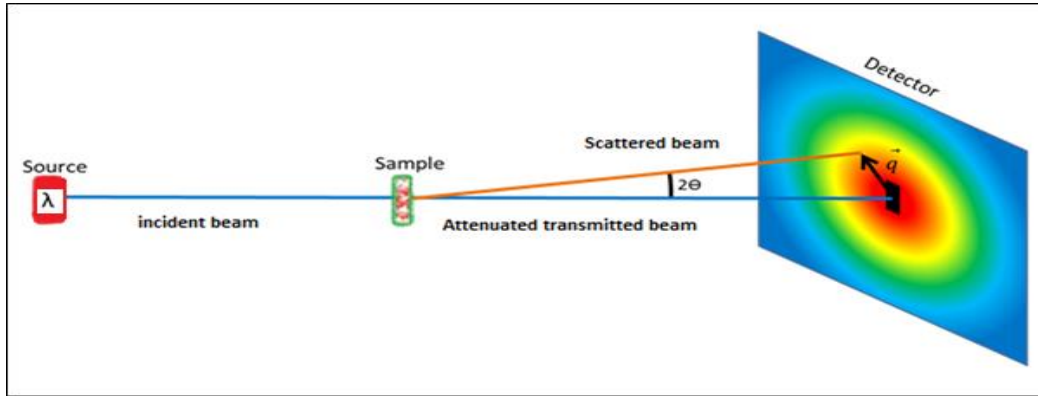


Figure 2-2: schematic illustration of a SANS instrument.

SANS setups is schematically illustrated in Figure 2-2. The neutron source is usually a fission reactor and the wavelength of incident neutron is fixed. As a result, the q is directly related to the scattering angle and by adjusting the distance between the detector and the sample different q will be scanned.

In SANS, the scattering intensity is recorded as a function of q , where q is the scattering vector and as described in equation (2-11):

$$q = \frac{4\pi}{\lambda} \sin(\theta) \quad (2-11)$$

where λ is the wavelength of incident beam and θ is the scattering angle. The q in SANS is analogous to the q in light scattering, and its value times R_g determines whether the sample is probed on local ($qR > 1$) or on global ($qR < 1$) length scale. The simplest description observed scattered intensity by the detector is shown below:

$$I(q) = K \times c \times P(q) \times S(q) \quad (2-12)$$

where K is a constant factor and consists of an instrumental factor, volume of particle and the difference between scattering-length densities of the medium and the sample. c is the mass concentration, $P(q)$ is the form factor and describes the geometry of the sample and $S(q)$ is the interparticle scattering term (structure factor) and describes correlation between particles mass centers [64, 65].

2.5 Nuclear magnetic resonance (NMR)

Nuclear magnetic resonance (NMR) offers a unique way of characterizing matter in all forms, ranging from solid materials like medicinal pills or catalysts to solutions of proteins, suspensions of living cells or even laboratory animals and human beings. NMR can be employed to study chemical (e.g. structure, conformational exchange) and physical (e.g. diffusion, hydrogen bonding, chemical exchange) properties of matters in liquid, solid or gas phase [66].

Every nucleus has mass and charge, but there is a third peculiar property that not all nuclei have, called spin. Unlike electrons that can have only $\frac{1}{2}$ or $-\frac{1}{2}$ spin, nuclei can have different spin quantum numbers depending on the number of protons and neutrons, and two isotopes of the same atom may have different spin numbers.

Among different nuclei, those which have spin quantum number $\frac{1}{2}$ (e.g. ^1H , ^{19}F , ^{13}C , ^{31}P , ^{15}N , ^{29}Si) are the most interesting nuclei to explore by NMR. In the presence of an external magnetic field, the nuclei with spin $\frac{1}{2}$ can possess only two positions (or two magnetic quantum numbers) aligned with magnetic field or against it. In absence of a magnetic field, both positions have the same energy; however inside the magnetic field there will be a splitting in the energy levels which is proportional to the strengths of the magnetic field (Figure 2-3). If the two populations are equal there will be no NMR signals. In NMR, all nuclei are not in the ground state and spins are distributed between the two energy levels with a little excess of population in ground state (partial polarization) [67, 68].

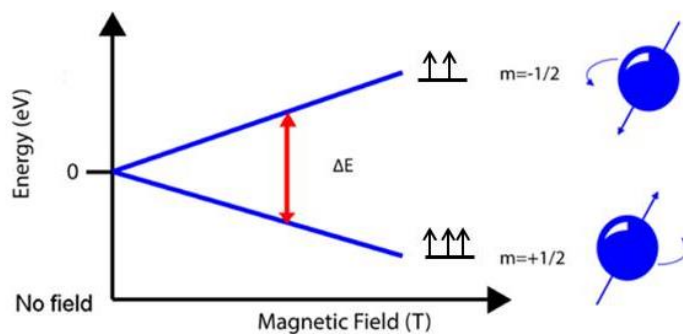


Figure 2-3: Energy level for a nucleus with spin quantum number $\frac{1}{2}$ in a magnetic field.

When performing a NMR experiment, the sample is immersed in a magnetic field to produce partial polarization. A radio frequency sender irradiates the sample to excite the partial nuclear spin difference in the ground state to the higher state. Then the radio sender is switched off, and the polarized spins will jump back to the ground state, emitting electromagnetic waves. This signal will be amplified further to display NMR signals. The electron cloud distribution around the nuclei in a molecule may alter due to the local environment around the nuclei, thus all same nuclei in a molecule or particle do not experience same magnetic field. This difference is called the chemical shift [67].

3 Experimental

The experimental methods are discussed in three sub-sections in this chapter. In the first section, synthesis of nanogels is described, the second part is devoted to the physical chemistry characterizations of synthesized nanogels, and the third is focused on biological evaluation of nanogels *in vitro*.

3.1 Synthesis

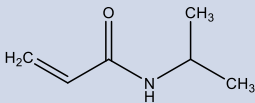
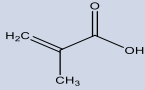
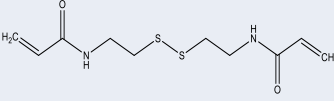
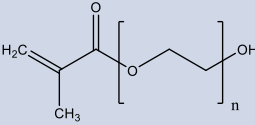
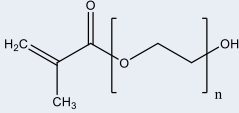
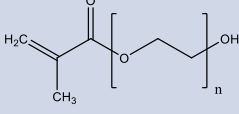
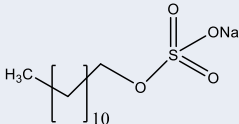
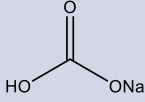
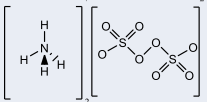
The nanogels have been prepared by emulsion polymerization in the presence of SDS, and 8 batches of different nanogels were synthesized successfully. The chemicals used during synthesis are listed in the Table 3-1.

3.1.1 Monomers purification

The monomers were purified prior to use to remove either impurities or inhibitors. N-Isopropylacrylamide (NIPAM) was recrystallized from a toluene/n-hexane mixture. Briefly, 50g of NIPAM was dissolved in 125 ml of toluene and heated for couple of minutes in a water bath, adjusted at 60°C. Then 250 ml n-hexane was added slowly while heating continued, the mixture then was cooled down first in the open air, and next cooled in an ice bath. The solution was left in refrigerator overnight to crystalize. The NIPAM crystals were extracted by filtration and dried in a vacuum oven. The initial NIPAM was off-white, while the final crystals were completely white.

Methacrylic acid was purified by distillation under reduced pressure to remove the inhibitor. A two necked "Claisen's flask" was used, the main neck was connected to a condenser and the other was attached to a thermometer. Claisen's flask was put in water bath that is adjusted on 60°C. The collection head was a 3-armed receiver (cow receiver) which allowed collecting the first (forerun), main and last run of condensed materials separately, while attached to vacuum pump (see Figure 3-1). First and last run was thrown away and main part were collected and stored at -24°C.

Table 3-1: list of chemicals that used for synthesis, and their specification.

Name	Structure formula	Abbreviation	Purity	Supplier	CAS No.
N-Isopropylacrylamide		NIPAM	≥ 97%	Sigma Aldrich	2210-25-5
Methacrylic acid		MAA	≥ 99%	Sigma Aldrich	79-41-4
N,N'-Bis(acryloyl)cystamine		BAC	≥ 98%	Alfa Aesar	60984-57-8
Poly ethylene oxide methyl ether methacrylate (2000)		PEGMA2000	---	Sigma Aldrich	26915-72-0
Poly ethylene oxide methyl ether methacrylate (5000)		PEGMA5000	---	Alfa Aesar	26915-72-0
Poly ethylene oxide methyl ether methacrylate (13000)		PEGMA13000	---	Alfa Aesar	26915-72-0
Sodium dodecyl sulfate		SDS	≥ 98.5%	Sigma Aldrich	151-21-3
Sodium bicarbonate		---	≥ 99.5%	Sigma Aldrich	144-55-8
Ammonium persulfate		APS	≥ 98%	Sigma Aldrich	7727-54-0
Sodium chloride	Na^+Cl^-	---	≥ 99%	Sigma Aldrich	7647-14-5

Poly ethylene oxide methyl ether methacrylate (average $M_w=2,000$, PEGMA-2000) was received as a 50% solution. Subsequently, it was freeze-dried before removing the inhibitor. Poly ethylene oxide methyl ether methacrylate ($M_w=5000$, PEGMA-5000) and Poly ethylene oxide methyl ether methacrylate ($M_w 13000$, PEGMA13000) were received as powders. All these monomers were purified by column chromatography. The procedure was as following: the monomers were dissolved in dichloromethane (DCM). The column was packed with alumina as stationary phase. The successful removing of the inhibitor residual was confirmed by 1H NMR.

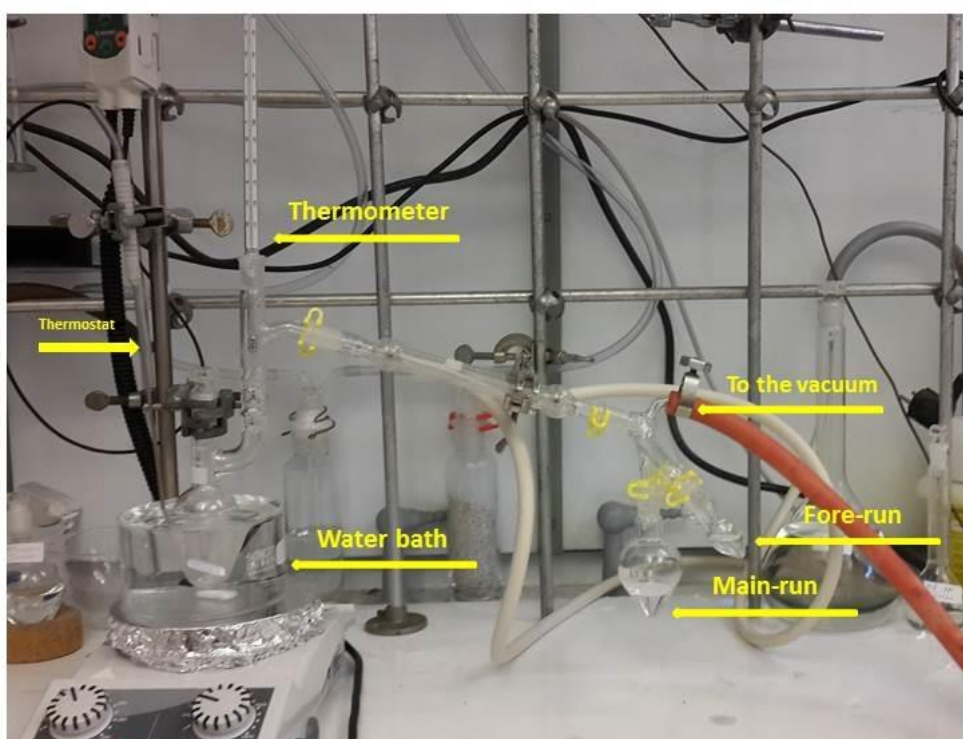


Figure 3-1: Vacuum distillation setup. A Claisen's flask was connected to a condenser. 3-armed receiver (cow receiver) used as a collector.

3.1.2 Synthesis of nanogels

The synthesis was carried out in 500 ml three-necked, round bottom flask with reflux condenser placed in the silicon bath. First argon was purged in the empty flask for 10 minutes. Then NIPAAM, co-monomer (MAA), Sodium bicarbonate and SDS were dissolved in 150 ml (1 wt. % to the monomers) MilliQ water (ultrapure water, conductivity=18 Ω M.cm) and filtered with 0.2 μ m Millipore regenerated cellulose filters. The solution was added to the reactor and purged with argon for 20 minutes before heating, while stirring vigorously with a magnetic stir (see Figure 3-2). The reactor contents then were heated up to 70°C while purging continued for 40 more minutes. Since BAC is insoluble in cold water, it was added during the heating process. 32 mg of APS (1 wt. % to the NIPAAM) was dissolved in 1 ml MilliQ water and degassed in a small vial with argon. The third connection of round bottom flask sealed with a septum, and degassed APS solution was injected immediately to initiate the reaction. The PEGMA oligomer was dissolved in 5 ml MilliQ water and degassed in a small vial. For the formation of PEGMA-rich shell, after 40 minutes of polymerization, the solution of PEGMA oligomer was added by auto-injection system in 5 minutes (Figure 3-3). The reaction was allowed to heat and stir for 6 hours while keeping the solution under argon atmosphere. Subsequently, heating was stopped, whereas stirring and argon flow continued over night to avoid any aggregation. In the next step, synthesized nanogels were dialyzed against MilliQ water for 4 weeks via a dialysis tube (SpectrumLab, molecular weight cut-off 50000) with the water being changed twice per day to remove any unreacted compounds. The samples were freeze-dried afterwards and collected for further experiments. The initial mole ratio of different reagent and resultant yield for each batch of synthesis are summarized in Table 3-2.

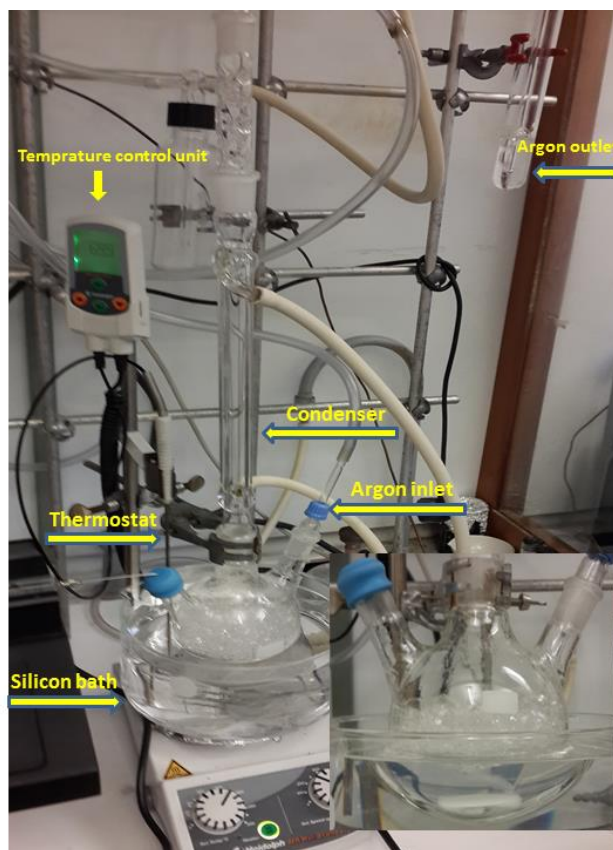


Figure 3-2: Synthesis reactor setup.

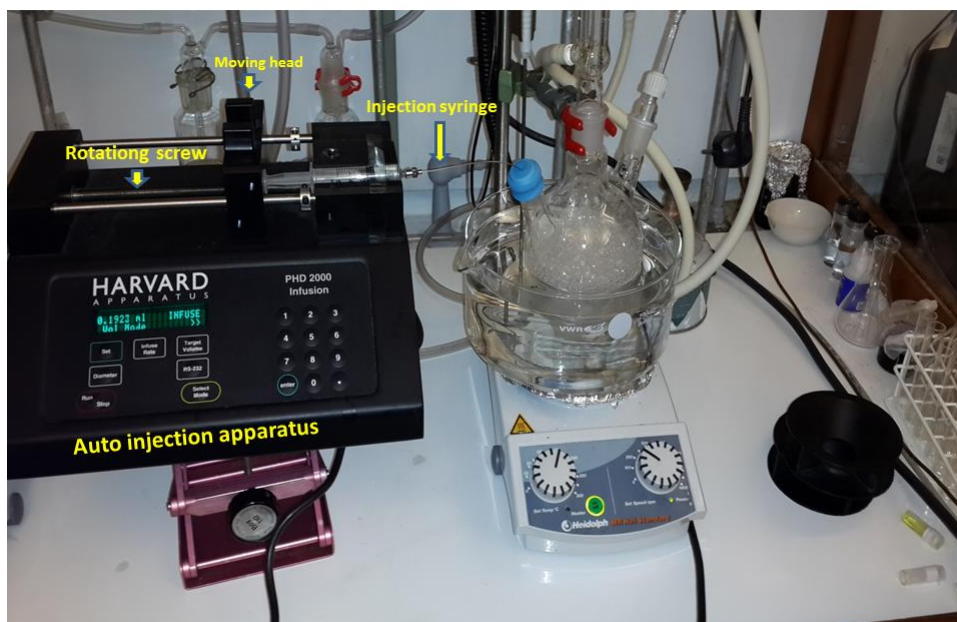


Figure 3-3: Auto injection apparatus setup for control addition of PEGMA to the reactor.

Table 3-2: List of synthesized nanogels

batch No.	NIPAAM (mole %)	Methacrylic Acid (mole %)	Cross-Linker (mole %)	SDS concentration (mg/ml)	PEGMA (Mw)	PEGMA (mole %)	Initiator (mole % of NIPAAM)	Coding system	Yield of polymerization
NG1	91	6	3	0.4	---	---	1	NG1	66 %
NG2	90.95	6	3	0.4	2000	0.05	1	NG2-2000-0.05	67 %
NG3	90.5	6	3	0.4	2000	0.5	1	NG3-2000-0.5	62 %
NG4	90	6	3	0.4	2000	1	1	NG4-2000-1	60 %
NG5	90.95	6	3	0.4	5000	0.05	1	NG5-5000-0.05	76 %
NG6	90.5	6	3	0.4	5000	0.5	1	NG6-5000-0.5	74 %
NG7	90	6	3	0.4	5000	1	1	NG7-5000-1	71 %
NG8	90.95	6	3	0.4	13000	0.05	1	NG8-13000-0.05	65 %

In this thesis, the effect of PEG length and PEG concentration, was studied by preparing nanogels in two different PEG lengths (2000 and 5000) in two different concentrations (0.05, 0.5 and 1 mole %). One more sample with PEG-13000 with concentration of 0.05 mole % percent was also prepared. In addition, one sample with no PEG layer was synthesized, resulting in eight different samples in total (see Table 3-2 and Figure 3-4). Following coding system was employed for identification of each sample: NG stands for nanogels, the first number after dash corresponds to PEG Mw and number after that is assigned to the corresponding mole % (e.g. NG2-2000-0.05, NG3-2000-0.5 and so on).⁵

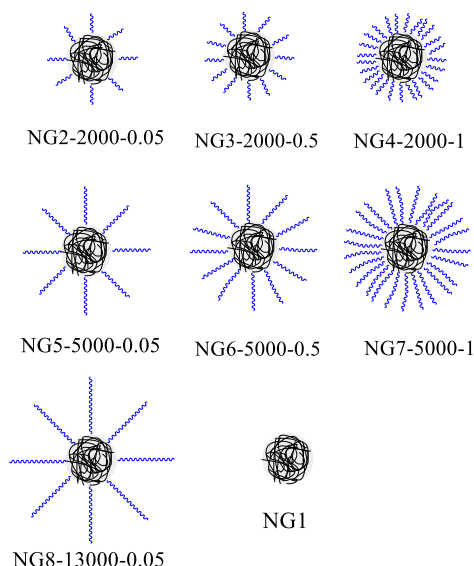


Figure 3-4: Schematic illustration of synthesized nanogels.

⁵ Due to the lack of space in some graphs the second part of nanogels names are omitted.

3.2 Physical chemistry methods

3.2.1 Dynamic light scattering (DLS)

The light scattering samples must completely be dust-free. Presence of dust leads to stronger scattering which can cause wrong correlation function. To prepare dust free-samples ca.2ml of the samples were filtered through a $0.8 \mu\text{m}$ filter (Millipore) into the pre-cleaned 10 mm NMR tubes inside a glove box. The tubes were rinsed with ethanol vapor prior to use (see Figure 3-5).

The DLS measurements were conducted using an ALV/CGS-8F multi-detector compact goniometer system with eight fiber-optical detection units made by ALV-GmbH, Langen, Germany. The intensity of scattered light measured simultaneously by eight detectors at eight different scattering angles ranging from 22° to 141° . The laser light (He-Ne, $\lambda = 632.5 \text{ nm}$) was focused on the 10 mm NMR tube. The measurement cell was cylindrical quartz container filled by a refractive index-matching liquid (*cis*-decalin) which was connected to a temperature control system.

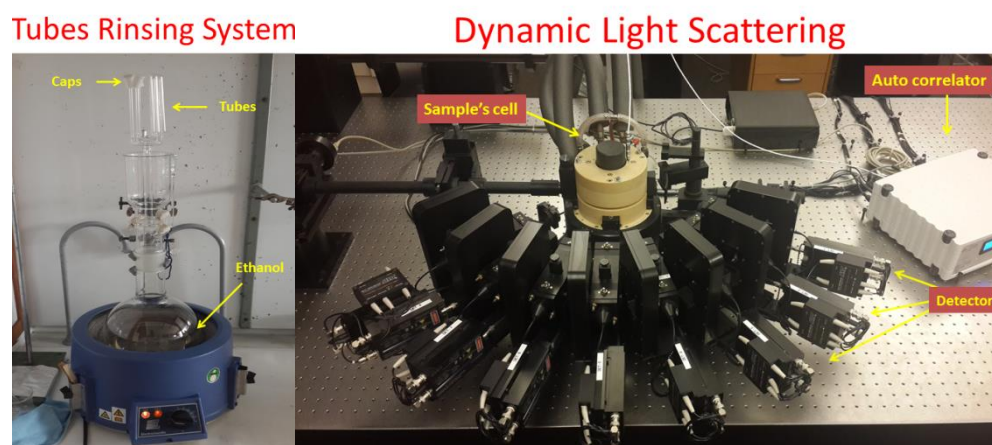


Figure 3-5: Picture of the tubes rising system (left) and the multi angle dynamic light scattering (right).

3.2.2 Small angle neutron scattering (SANS)

All the SANS measurement were conducted at the Institute for Energy Technology (IFE, Kjeller). The neutron source was the JEEP-II reactor, and two different detector distances (1.0 and 3.4m) and two different neutron wavelengths (5.1Å/10.2Å) were used in order to obtain a largest possible q-range range.

The transmission was measured separately, and the scattering was normalized to absolute units (cm⁻¹) by taking into account an empty cell and the general background scattering. The measurement cell was 2 mm quartz cuvettes, and the sample was prepared in *D*₂*O* at 25°C, and inspected before being introduced into the cell.

The prepared samples were sent to the Institute for Energy Technology (IFE), and the measurements and fitting were performed by Dr. Kenneth Dahl Knudsen.

3.2.3 Turbidimetry

The turbidity measurements were performed on a NK60-CPA could point analyzer (Phase Technology, Richmond, B.C., Canada). The source of light was an AlGaAs laser with wavelength of 654 nm, and 18 nm spectra width. Turbidity of the samples was directly measured as signal intensity over a temperature range of 25-45°C. The instrument was provided with a glass plate covered with a thin metallic layer of very high reflectivity mirror. 150 µL of the dispersion was added by a micropipette on the top of glass plate, the sample then was covered with 150 µL of highly transparent silicon oil in order to prevent solvent evaporation. The temperature was probed by a platinum resistance thermometer, and a thermoelectric device was utilized to adjust the temperature over range of -60 to +60°C. The heating rate was set to 0.5°C/min, and lower heating rate had no effect on observed signal.

3.2.4 Zeta potential

The zeta potential measurements were carried out on a Zeta-sizer Nano ZS (Malvern Instrument Ltd. Worcestershire, UK). The sample cell was composed of a 10 mm PMMA cuvette, a “dip-cell”, palladium electrode with 2 mm spacing and a cap. The electrophoretic mobility of

the sample was determined via Laser Doppler Velocimetry (LDV) by the instrument. Every set of experiments was started with measuring the standards solution of -42 mV in triplicate. Subsequently, each sample was measured three runs by measuring 600 μL of each sample, to ensure repeatable results.

3.2.5 ^1H NMR

^1H measurement was performed on Bruker Avance AV 600 MHz NMR spectrometer operating at 600.13 MHz (^1H) with inverse cryoprobe, equipped with a Z-gradient coil. The data were processed afterward by Bruker TOPSPIN (version 3.5p17) software. The ^1H NMR data were obtained at 25°C by 256 scans. All samples were prepared in D_2O , and 600 μL of each sample was filled in the 5 mm NMR tubes and sealed with a cap.

3.3 Biological experiments

All nanogels were colored by coumarin-6 for biological assay via following procedure. A 50 μL solution of 1 mg/mL coumarin-6 in dimethylformamide (DMF) was added to solution of the nanogels (0.5 wt. % in MilliQ H_2O). The mixture was centrifuged three times (Eppendorf 5430R, at 17500 rpm), supernatant was discarded and replaced with MilliQ water. The final concentration was adjusted to 50 $\mu\text{g}/\text{mL}$ for further experiments. In this regard, *in vitro* cytotoxicity and macrophage uptake conducted on the samples to give picture about their biological behavior.

The prepared samples were sent to the cancer research institute located at Norwegian Radium Hospital, (Oslo University Hospital, Norway), and the experiment was performed by my co-supervisor Dr. Shahla Bagheri Fam.

3.3.1 *In vitro* cytotoxicity

MDA-MB-231 breast cancer cells (ATCC- American type culture collection) were cultured in RPMI 1640 cell culture medium (Lonza, Verviers, Belgium) containing 10% fetal bovine serum and 1% penicillin–streptomycin (Sigma), and then seeded in 96-well plates at the density of 5000 cells/well. Plates were incubated at 37°C in humidified atmosphere with 5 % CO_2 . 24 hours post

incubating cells were treated with 200 μ L fresh cell culture medium containing the PEGylated and non-PEGylated nanogels in three different concentrations (5, 15, 25 μ M). The control group was treated with only fresh cell culture medium. Following the treatment period, cell viability was determined using the MTS (3-(4,5-dimethylthiazol-2-yl)-5-(3-carboxymethoxyphenyl)-2-(4-sulfophenyl)-2H-tetrazolium) assay according to manufacturer's instruction. Briefly, 100 μ L of MTS was added to each well and cells were incubated for 3 h. The absorbance of formazan at 490 nm was measured in a colorimetric assay with an automated plate reader (Victor Wallac 2, Perkin Elmer). Six wells were designated for each sample and the average cell viability was calculated as below equation:

$$\text{Cell viability} = \frac{\text{mean absorbance of treated wells} - \text{blank}}{\text{mean absorbance of control wells} - \text{blank}} \times 100 \quad (3-1)$$

3.3.2 Macrophage uptake

THP-1 human acute monocyte cells were cultured in RPMI 1640 cell culture medium (Sigma) containing 10% fetal bovine serum, 1% penicillin-streptomycin and 2-mercaptoethanol (0.05 mM).

THP-1 cells were seeded (15000 cells per well) in 8-well glass slide and induced to differentiate into macrophages by adding 200 μ L culture medium containing 50 nM phorbol 12-myristate 13-acetate (PMA) and incubated at 37°C with 5% CO₂. After 48 hours the macrophages were treated by fresh culture medium containing PEGylated and non-PEGylated nanogels (15 μ g/ml). Treated macrophages were incubated for 6 hours, washed two times with PBS and fixed by paraformaldehyde (4%) and visualized by a confocal microscopy. For better visualization of the cells, nuclei were stained with DAPI (2-(4-Amidinophenyl)-6-indolecarbamide dihydrochloride). Cell imaging was conducted utilizing a confocal microscope (Zeiss LSM 710) equipped with Plan-Apochromatic 63 \times 1.4 NA oil immersion objective (Zeiss-Germany).

4 Results

4.1 Synthesis of PEGylated poly (N-Isopropylacrylamide-co-methacrylic acid)

The synthesis was performed according to the procedure described in 3.1.2 subsection. The reaction and presumed chemical structure of the PNIPAM-co-PMAA-co-PEG system is illustrated in Figure 4-1. The successful polymerization of NIPAM and MAA was confirmed by 1H NMR. Figure 4-2 shows the 1H NMR spectrum of NG2-2000-0.05 as an example. 1H NMR results from all other synthesized nanogels are provided in appendix I. The chemical shifts are shown on structure formula of the nanogels. The chemical shifts at $\delta=1.07$ (peak a) and 3.83 (peak b) ppm are well resolved and correspond to hydrogen atoms of methyl and methine groups of NIPAM, respectively. Moreover, amide hydrogen is observed as peak "c" ($\delta=7.64$ ppm), which is difficult to detect since the amide peaks tend to broaden into the baseline. The MAA peaks are merged into NIPAM peaks, while the PEGMA characteristic peak "i" ($\delta=3.63$ ppm) are quite distinct in the spectrum. No characteristic peak corresponding to BAC was detected, suggesting a structure in which BAC is in the core of the nanogel. Other chemical shifts corresponding to polymethacrylic acid and $-CH_2$ groups are in accordance with previous studies [44, 69, 70].

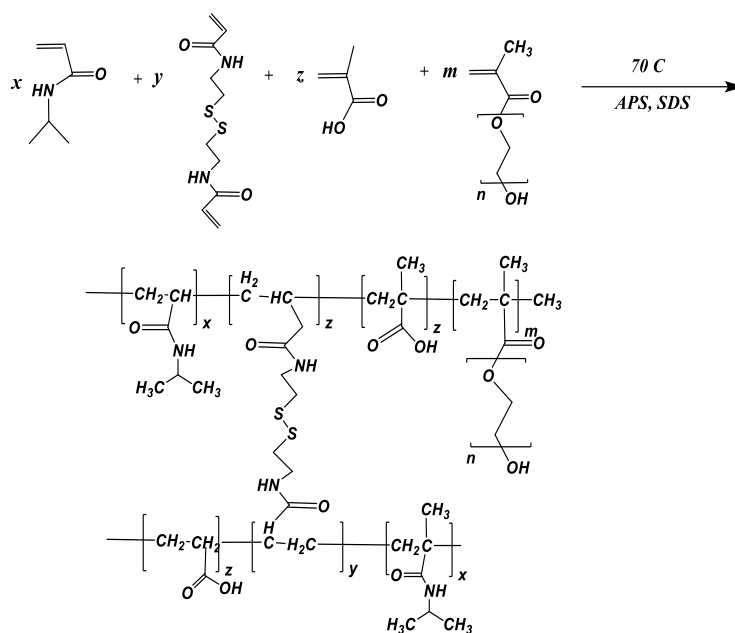


Figure 4-1: Schematic illustration of the synthesis and chemical structure of the cross-linked PNIPAM-co-PMAA-co-PEG nanogel system.

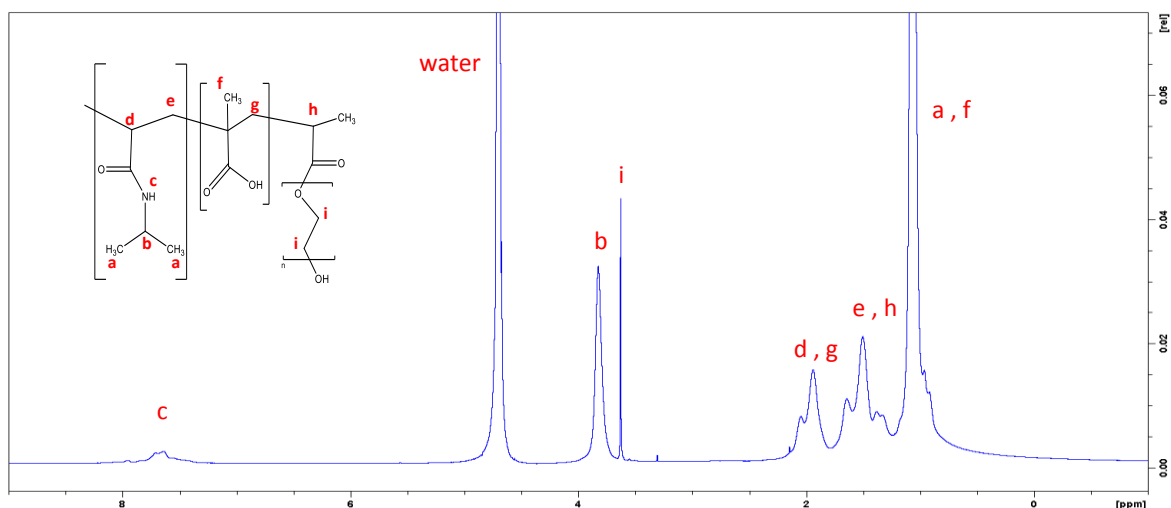


Figure 4-2: ^1H NMR spectra of NG2-2000-0.05.

The area under each peak in ^1H NMR spectrum is proportional to relative number of equivalent protons. Therefore, by integrating one of the peaks which corresponds to NIPAAm and the PEG, the resultant molar ratio of PEGMA can be calculated, assuming all other reagents are consumed completely. Peak “b” is a good choice for calculating this ratio since it is generated only from NIPAAm’s hydrogen and is not merged with other hydrogens. On the other hand, since peak “i” is only assigned to PEGMA’s methylenes group and because the molecular weight of PEGMA is known, the relative molar ratio of PEGMA can be determined. The data for initial and resultants nanogels molar ratio of PEGMA oligomers are summarized in Table 4-1. The calculations are described in details in appendix I.

Table 4-1: Initial PEG mole % of synthesized nanogels vs. final PEG mole % of nanogels (after dialysis) that calculated from NMR.

Nanogels	Initial molar ratio (mole % of PEGMA)	Resultant molar ratio from NMR (mole % of PEGMA)
NG1	---	---
NG2-2000-0.05	0.05	0.08
NG3-2000-0.5	0.5	0.56
NG4-2000-1	1	0.99
NG5-5000-0.05	0.05	0.07
NG6-5000-0.5	0.5	0.58
NG7-5000-1	1	1.11
NG8-13000-0.05	0.05	0.06

4.2 Zeta potentials

To investigate the surface charge of the systems, a zeta potential measurement was performed on different nanogel systems. The measurements were conducted on 1 wt. % nanogels dispersion in ultrapure water and 2 mM solution of SDS. In addition, by measuring the zeta potential at four different temperatures (25, 30, 35 and 40°C) the effect of temperature on the surface charge of the systems was studied.

The zeta potential results for samples in pure water over range of temperature 25-40°C are illustrated in Figure 4-3. These nanogels are expected to be negatively charged due to the presence of COOH group from MAA monomer and sulfate group from the initiator. At 25°C, zeta potential of nanogels ranges from -10 to -7 which are quite low for electrostatic stability. As the temperature increased, a higher negative zeta potential value was observed. At higher temperature, the PNIPAAm chains become hydrophobic, causing the nanogels to shrink. When temperature reaches to the LCST, the PNIPAAm chains collapse, and the core condenses, causing the charged group to be expelled from the core which leading to an increase in the absolute value of zeta potentials.

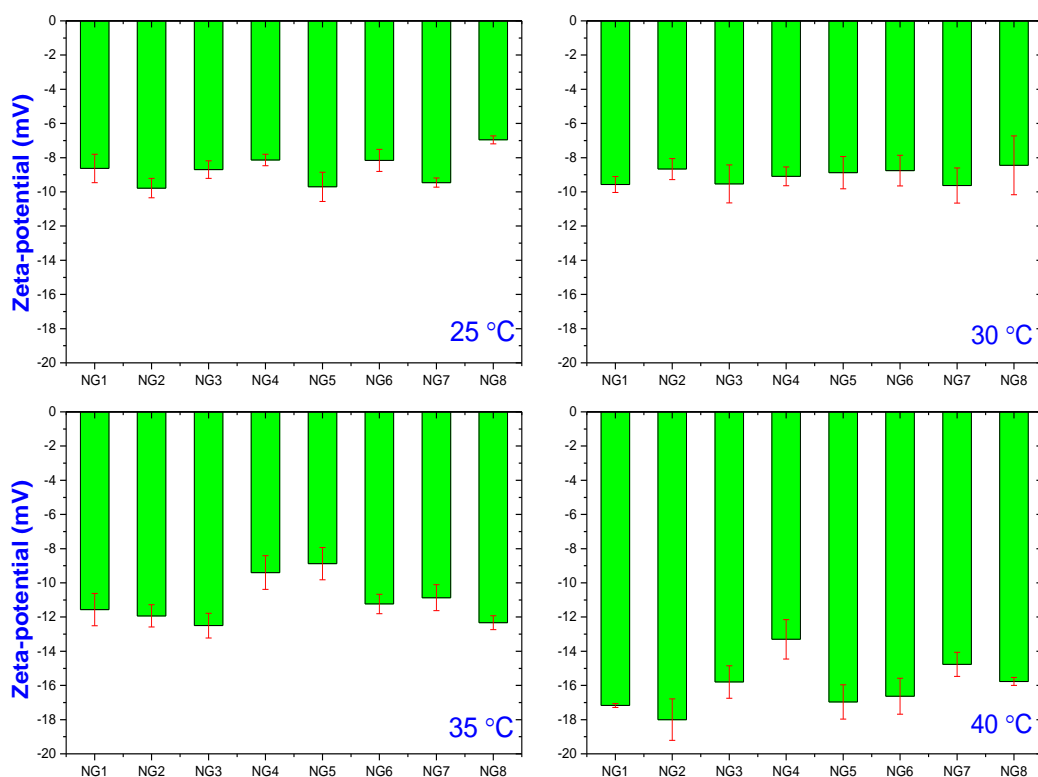


Figure 4-3: Zeta potential of 1 wt. % samples in ultrapure water at different temperatures.

To investigate the effect of SDS on the zeta potential of nanogels, the nanogels were dispersed in 2 mM SDS solution to reach a final 1 wt. % concentration. The zeta potential was measured at for different temperature (25, 30, 35 and 40°C), Figure 4-4. A comparison between Figure 4-3 and Figure 4-4 indicates that by adding SDS, absolute zeta potential values at all four different temperatures slightly increases. This might be explained by possible absorption of SDS molecules on the surface of nanogels which increases the surface charge.

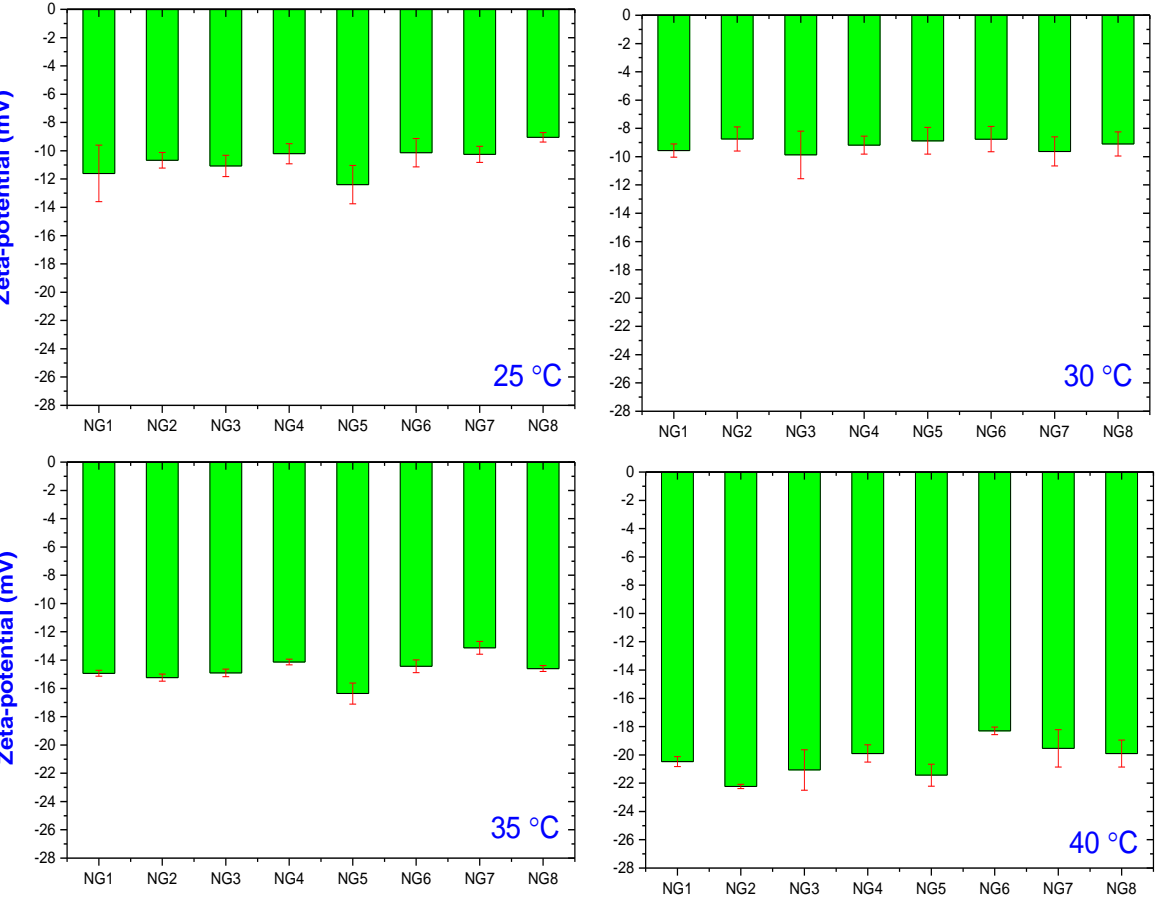


Figure 4-4: Zeta potential of 1 wt. % samples in 2 mM SDS solution water at different temperatures.

4.3 Turbidimetry

The turbidimetry measurement is a valuable method to monitor the transition temperature of temperature responsive nanogels, by monitoring the major changes in turbidity of a sample. A sharp increase in turbidity curve indicates development of hydrophobic association, which is referred to as cloud point (CP). In this study, PNIPAAm is the main building component of nanogels which has LCST around 32°C and tends to phase separate at temperatures higher than this point [71]. Temperature responsivity of the synthesized nanogels was studied both in pure water and sodium chloride solution. For each nanogel two samples with 1 wt. % and 2.5 wt. % were prepared in water, whereas for the saline solution only 1 wt. % samples were prepared in three different salt concentrations (0.01M, 0.05M and 0.1M). In this chapter mostly results from nanogels with PEG-2000 layer are discussed, however the conclusions can be extended to the samples with higher PEG length.

Turbidity of 1 wt. % nanogels dispersion in pure water with different PEG-2000 surface concentration and NG1 (without any PEG) are illustrated in Figure 4-5-a. Some of the 1 wt. % samples do not show the sharp turning points, probably due to low concentration which did not allow them to form large enough associations. However, by zooming into the plots and considering the points at which turbidity is lifted from the baseline, CP can be determined (see Figure 4-6). It is clear that the CP shifted towards higher temperatures as the concentration of PEG-2000 increases. This increase in CP is probably associated with steric stabilization caused by the anchored PEG layer. The height of the signal is proportional to turbidity of the samples; the higher signals indicate higher turbidity level of the samples. NG1 sample that has no PEG layer, shows stability to some extent at 1 wt. % dispersion at 25°C (cloud point=28°C). The reason that it does not form aggregates at this temperature is probably due to the slight charge density (stems from -COOH group of MAA and -SO₄⁻ from initiator) at its surface which was confirmed by zeta potential measurements (section 4.2).

The turbidity of PNIPAAm is a function of both temperature and concentration [71]. In order to study the effect of concentration all nanogel samples were prepared in 1 wt. % (Figure 4-5-a) and 2.5 wt. % (Figure 4-5-b) dispersion. It is clear that the concentration of the sample is a crucial parameter that influences both CP and signal intensity (turbidity). The CP of high PEG

content nanogels (NG4-2000-1) is dramatically shifted toward lower temperatures, while the decrease in CP is less significant for the samples with a lower PEG content. By increasing the concentration of nanogels in dispersion, the collision frequency and sticking probability would increase. As a result, formation of aggregates occurs at lower temperatures, leading to a decrease in the CP. The increase in turbidity of more concentrated samples may occur due to the formation of bigger clusters. As the aggregates become bigger, they scatter light more intensely, resulting in the higher detected signals.

The other interesting parameter investigated in this work, is the effect of PEG length on turbidity. A comparison between three nanogels with equal PEG surface concentration and various PEG lengths was studied (Figure 4-5-c). For all samples turbidity increases with temperature except for nanogels with the highest PEG length (PEG-13000).

In Figure 4-5-c, turbidity of nanogels with PEG-13000 decreases by increasing the temperatures. By increasing the temperature, PNIPAAm becomes more “sticky”, since the hydrophobicity of PNIPAAm increases. At the cloud point, PNIPAAm becomes enough hydrophobic to form intermolecular associations, and the nanogels form bigger particles on collision. Further increase in hydrophobicity with temperature causes the interactions between PNIPAAm and water to become less favorable (poor solvent) and PNIPAAm chains associate themselves in way to have the least contact with water, resulting in contraction of the particles. Thus, at elevated temperatures there is a competition between aggregation and contraction. In presence of enough protection by different mechanisms (here steric stabilization by PEG chains), nanogels are prevented from forming bigger association while the size decreases due to the contraction. A decrease in hydrodynamic radius of the nanogel with a PEG-13000 layer at highest temperature (40°C) was observed by DLS. Consequently the turbidity declines at higher temperature for this sample.

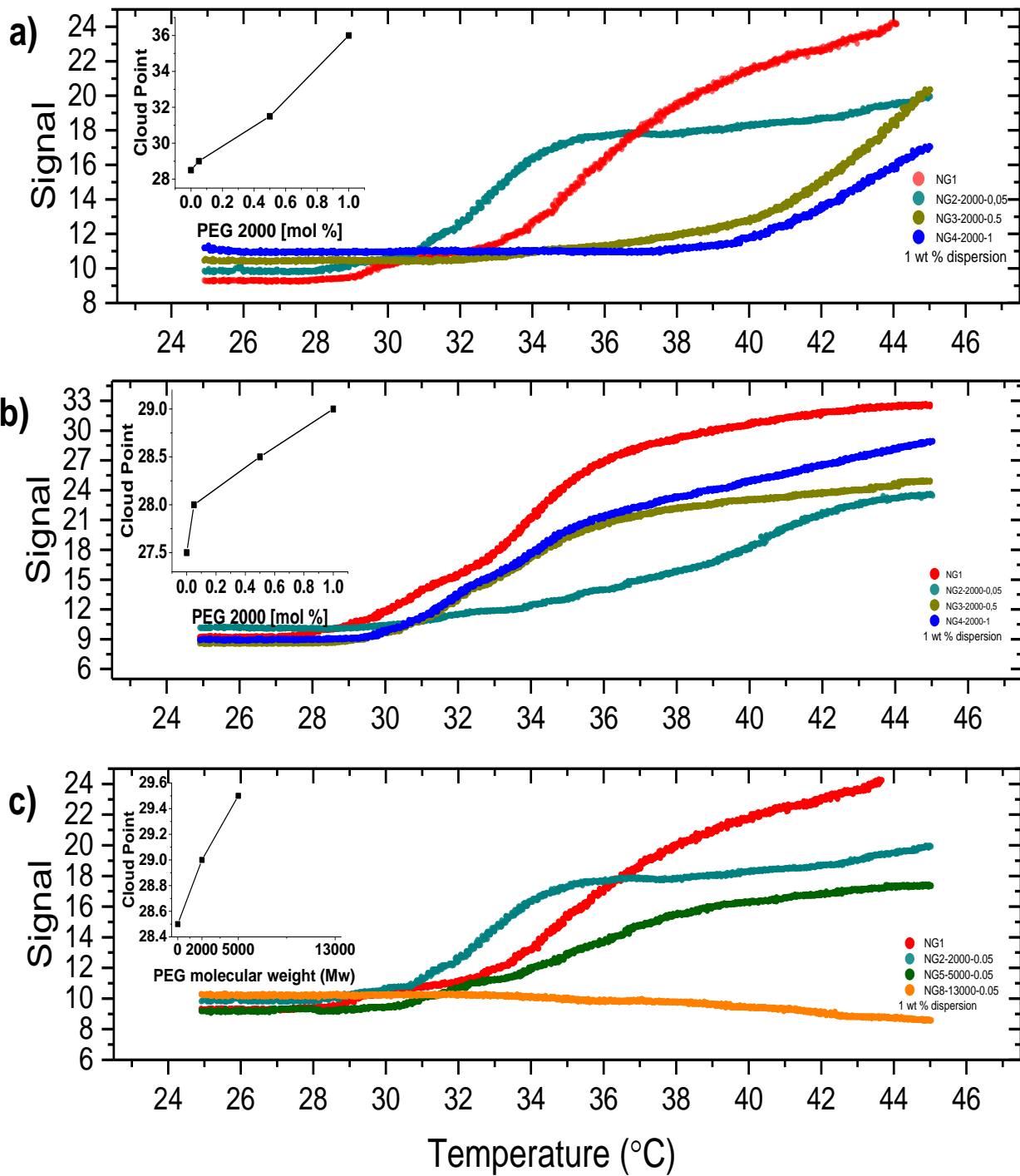


Figure 4-5: a) The turbidity result of nanogels with different concentration of PEG 2000 and without PEG layer. b) The turbidity result of 2.5 wt. % dispersion of nanogels with different concentration of PEG layer and the one without any PEG layer. c) The turbidity result for NG1 (without PEG) and three 1 wt. % nanogels with the same surface concentration of PEG with various PEG lengths. The corresponding cloud point are shown in the inner plots.

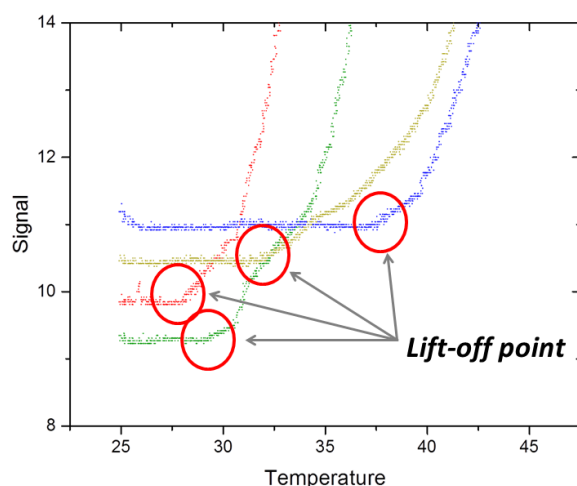


Figure 4-6: The zoomed turbidity curve, the lift-off points are marked with red circles. In lift-off point the turbidity curves arises from baselines, the corresponding temperature is registered as the cloud point (CP).

The other parameter that can affect the turbidity is the ionic strength. This effect was investigated by dispersing nanogels in saline solution. 1 wt. % nanogel dispersions in three saline solutions (0.01M, 0.05M and 0.1M) were prepared and the turbidity was measured (Figure 4-7-a). The CP declined by adding more salt while turbidity increased and the transition zone is more distinct. As the salt concentration increases, screening of electrostatic charges by the salt ions becomes more efficient and the effective EDL length decreases. In this study salt concentration as low as 0.01M can increase the turbidity of the systems and shift the CP to lower temperatures by screening the electrostatic charge. At higher salt concentration (0.1M), electrostatic interactions should virtually be screened or very weak [53]. Due to the Hofmeister effect, higher salt concentrations may increase the hydrophobicity of PNIPAAm-co-MAA chains and nanogels become more sticky [53]. This caused the turbidity (signal) to rise to higher values and CP shifted towards lower temperatures.

Figure 4-7-b shows turbidity of the samples with the same PEG surface concentration (0.05 mole %) and different PEG length (2000, 5000 and 13000). Results from one sample with no PEG layer was also included (NG1). The figure confirms that at high salt concentration PEG 2000 and 5000 has no effect in preventing aggregation, showing almost the same turbidity profile as NG1. Turbidity also increases for PEG-13000; however, this increase is much less than two other nanogels (with PEG 2000 and 5000 layer). This indicates that PEG-13000 can offer some extend of protection against aggregations even at high saline concentration.

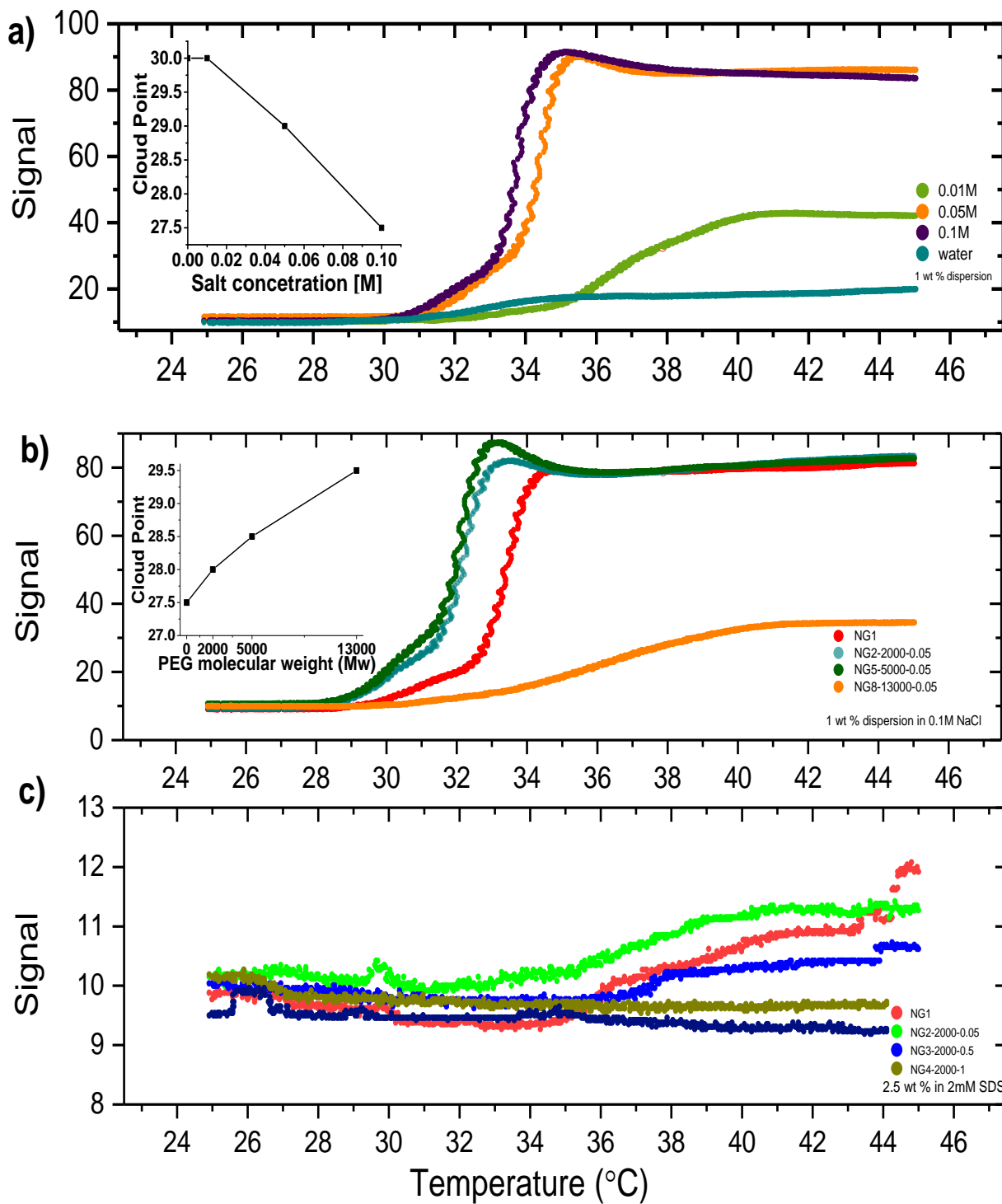


Figure 4-7: a) Turbidity curves for 1 wt. % dispersion of NG2-2000-0.05 at different ionic strength. b) Turbidity vs temperature of samples with 0.05 mole % PEG with three different PEG lengths. Also the NG1 (without PEG) illustrated as the grey curve. c) Turbidity of 2.5 wt. % dispersion of sample in 2mM SDS solution.

In this study, some complementary turbidity measurements were performed by adding SDS. Figure 4-7-c illustrates the turbidity measurement for 2.5 wt. % nanogels dispersion of NG1, NG2-2000-0.05, NG3-2000-0.5 and NG4-2000-1 samples in 2mM SDS solution. The results indicate that adding SDS can prevent aggregation to a large extent. Since the zeta potential value for samples with and without added SDS was approximately the same, electrostatic repulsion is probably not the dominant stabilization mechanism. The mechanism preventing the nanogels to form aggregates is probably the solubilization of the hydrophobic moieties. Pamies et al. has previously showed that presence of SDS at low concentrations can solubilize the PNIPAAm block [72]. Cloud points for each nanogel at different conditions are summarized in appendix II.

4.4 Dynamic light scattering (DLS)

DLS was employed to investigate the hydrodynamic radius of nanogels over the range of 25 to 40°C in temperature. Each sample was measured in two different media (ultrapure water and 2 mM SDS solution) with final concentration of 1 wt. %. Figure 4-8-a displays the first order electric field autocorrelation function $g^1(t)$ vs time at different angles for NG1 sample. The data were fitted with unimodal stretched exponential. The diffusion coefficient was calculated from the slope of the plotted decay rate (τ^{-1}) vs. q^2 (the inner graph) according to the equation (2-7). Subsequently, by using this diffusion coefficient in Stokes-Einstein (equation (2-8) relation, the hydrodynamic radius (R_h) was obtained. The stretching parameter " β " being close to 1 is an indication of a system with low polydispersity.

In order to obtain the R_h by DLS, it was presumed that the systems are diffusive and the relaxation modes are proportional to the mutual diffusion coefficient, meaning the decay rate (τ^{-1}) is q^2 dependent. In a diffusive system diffusion, the coefficient is independent of the scattering angle [61]. The diffusivity of the system was examined by plotting $g^1(t)$ vs. q^2t at different angles. The condensation of curves on the top each other discloses that the system is diffusive (see Figure 4-8-b).

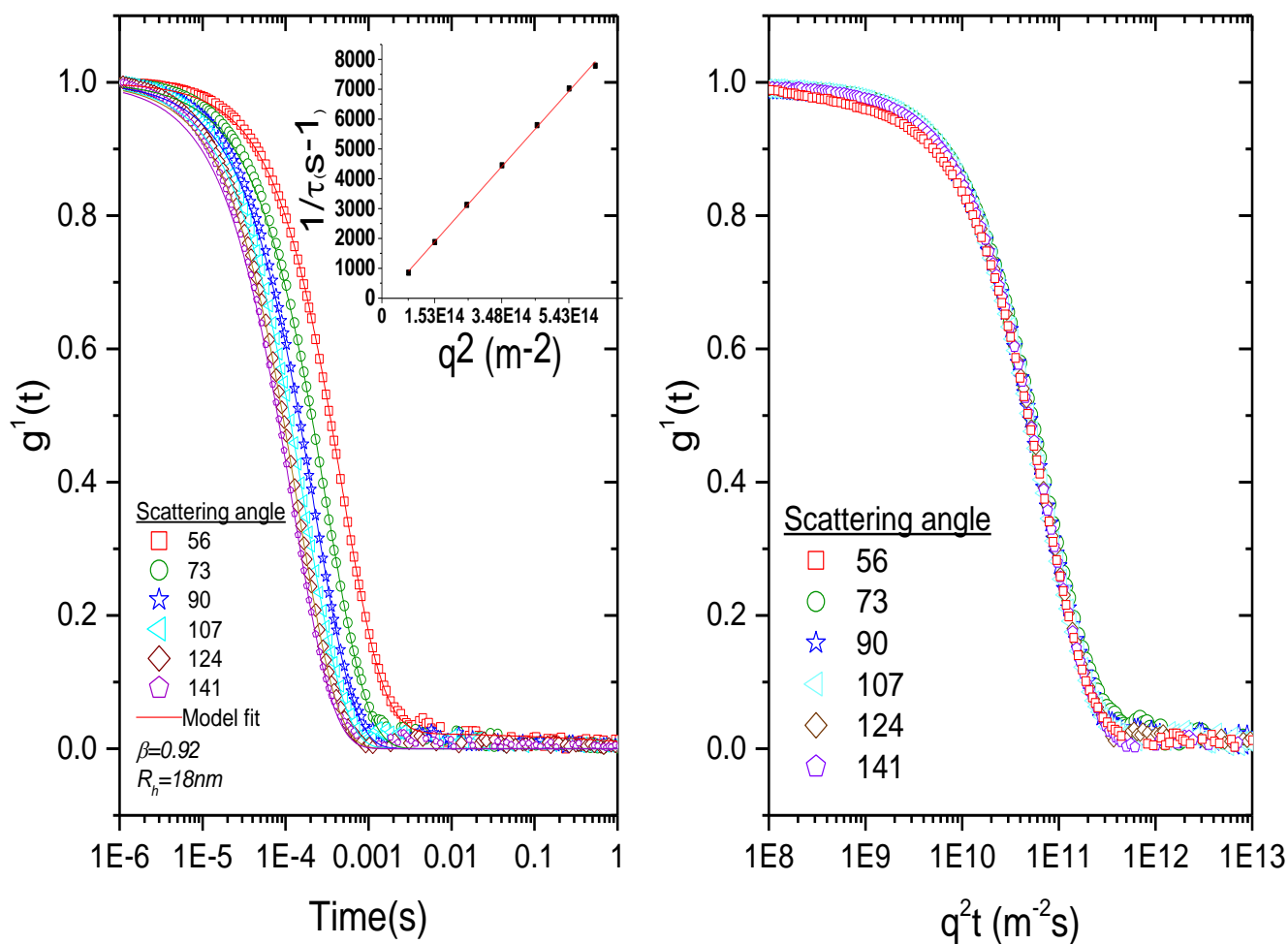


Figure 4-8: a) First electric autocorrelation function versus time and their corresponding fits of 1 wt. % NG1 in water at 25°C. The inset plots illustrates the inverse of decay rate (τ^{-1}) vs. q^2 . b) First order electric field autocorrelation function vs. q^2t for NG1 sample at 25°C. The β values calculated mean values with standard deviation of ± 0.02 .

In order to inspect the quality of the fit, the random distribution and small value of the residuals are plotted for each angle (illustrated in the inner graph of Figure 4-9). This shows no sign of systematic residuals which indicates the high quality of the fit.

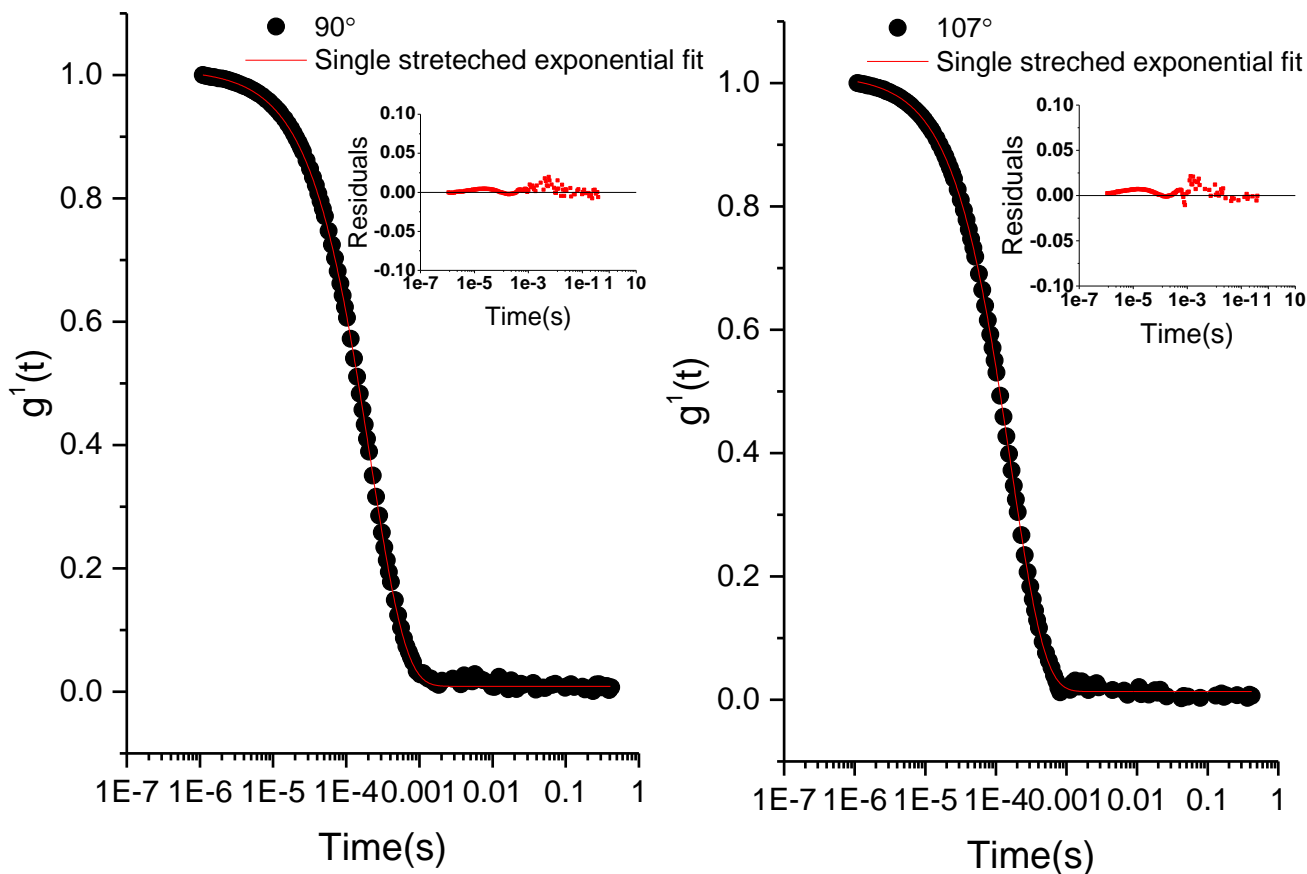


Figure 4-9: First order electric field autocorrelation function vs. time of NG1 sample at angle 90° (left) and 107° (right), and their corresponding fit. The residuals of each fit are shown in the inset plots.

To check the size temperature dependency of the nanogels, the $g^1(t)$ of 90° angle of each sample was plotted at different temperature. The Figure 4-10 shows this plot for the NG1 sample. It can be seen from Figure 4-10 that size of the sample become bigger at elevated temperatures. The fitted decay rate (τ^{-1}) vs. q^2 for NG1 are illustrated in Figure 4-10. It is clear that with increasing the temperature R_h also increase, while the β decreased at same time. NG1 has no PEG layer to protect it from aggregation, so the increase in size by aggregation for this sample was expected. The reduction in β values is an indication of increase in polydispersity of the system, suggesting that aggregation occurs at higher temperature. As it can be seen in Figure 4-10 some points deviate from the straight line at 35 and 40°C suggesting also a more polydisperse system.

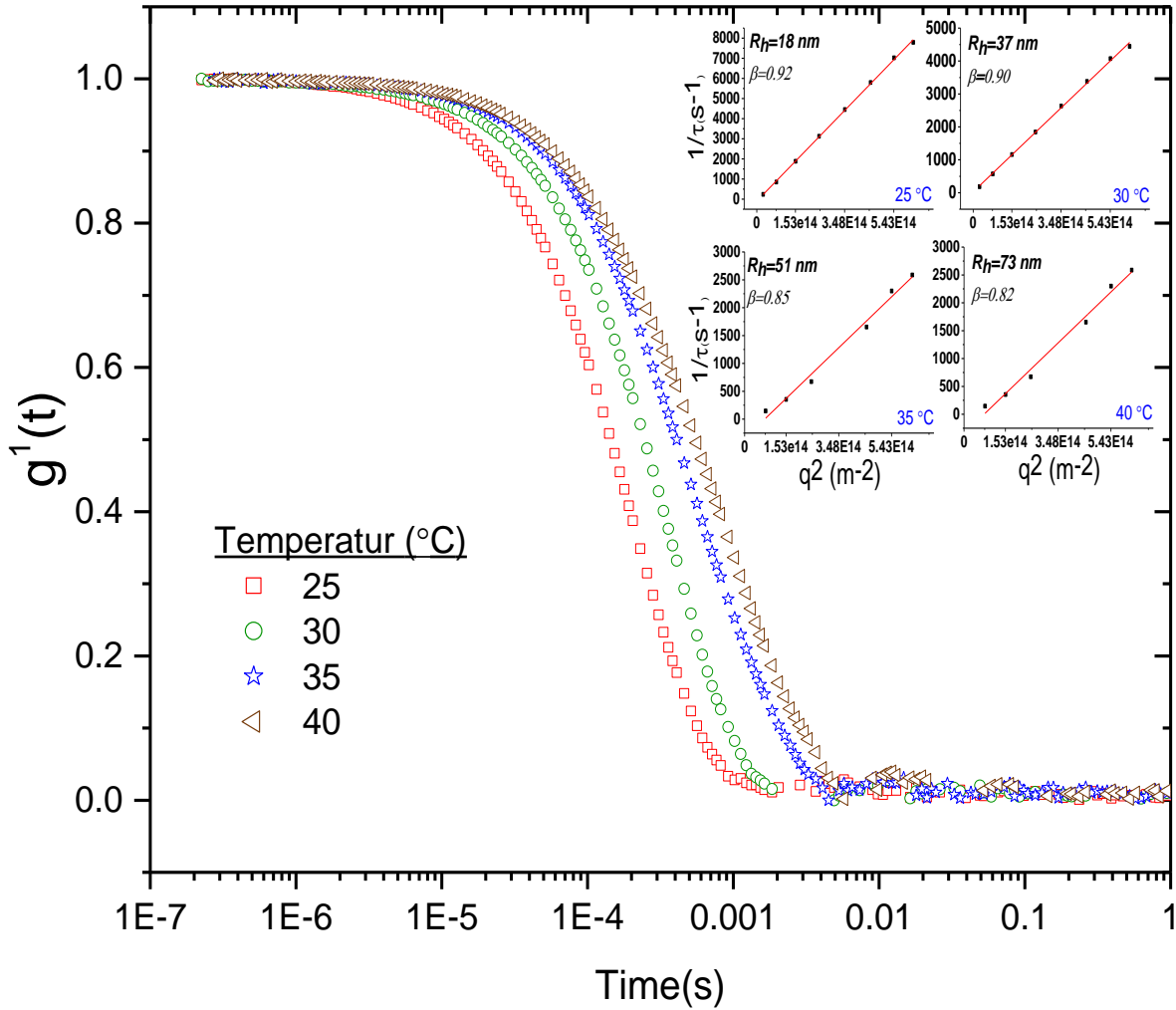


Figure 4-10: First electric autocorrelation function vs. time of NG1 sample at angle 90° at for different temperatures. The inset plots show the inverse of decay rate (τ^{-1}) vs. q^2 of 1 wt. % NG1 in water at four different temperatures (25, 30, 35 and 40°C). The β values are calculated mean values with standard deviation of ± 0.02 .

The hydrodynamic radii and the corresponding β values for the PEG-2000 coated nanogels with various surface concentrations are plotted versus temperature in Figure 4-11-a. At 25°C , R_h values increase slightly as the PEG surface concentration increases. The hydrodynamic radius of NG2-2000-0.05 shows the same behavior as the nanogels without any PEG coating and monotonically increases with temperature. This suggests that PEG-2000 at 0.05 mole % did not protect nanogels against aggregation. Nanogels with PEG-2000 at lowest surface concentration (0.05 mole %) showed a decrease in size at higher temperatures in comparison with nanogels without any PEG coatings (NG1). This shows that coating nanogels with PEG even at lowest concentration can prevent aggregation to a small extent. Further increase in surface

concentration of PEG-2000 (0.5 and 1 mole %) decreased the hydrodynamic radius of nanogels in comparison to nanogel without any PEG coating (NG1), suggesting more stable systems.

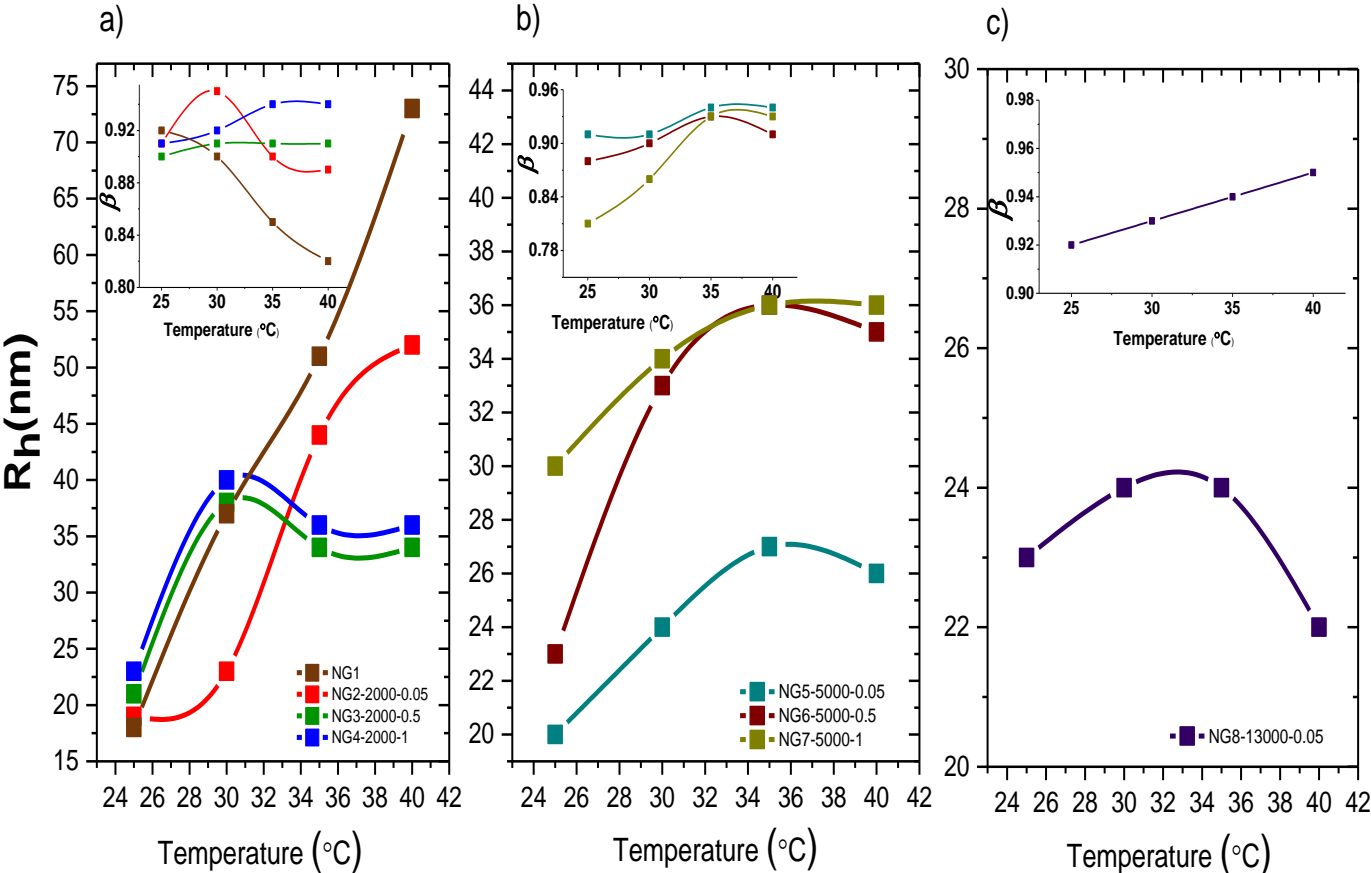


Figure 4-11: a) Hydrodynamic radii of NG1 (without any PEG layer) and PEG-2000 coated nanogels with 0.05, 0.5 and 1 mole % PEG surface concentration vs. temperature. b) Hydrodynamic radii of PEG-5000 coated nanogels with 0.05, 0.5 and 1 mole % PEG surface concentration vs. temperature. c) Hydrodynamic radii of PEG-13000 coated nanogels with 0.05 mole % PEG surface concentration vs. temperature. The corresponding beta values obtained from DLS are illustrated in inner plots. The β values calculated mean values with standard deviation of ± 0.02 .

Figure 4-11-b shows the temperature dependency of hydrodynamic radii and corresponding β values of nanogels with PEG 5000 layer. It can be seen from Figure 4-11-a that nanogels with PEG 5000 tend to form aggregates and they become larger as the temperature approaches the cloud point. Further heating causes the PNIPAAm chains to collapse above the LCST, as a result, their size reduces due to contraction of the systems.

For the nanogel with PEG 13000 layer the hydrodynamic radius slightly grows with the temperature (about 2nm) up to 35°C, but at 40°C the R_h becomes even smaller than R_h at 25°C (Figure 4-11-c). This suggests that this sample is fairly stable against aggregation. β values increase for both nanogels with PEG 5000 and 13000 at elevated temperature which again implies that the systems have lower polydispersity at higher temperatures. In appendix IV size distribution of different nanogels were investigated with AF4.

Adding SDS to the nanogels dispersion increases their surface charge slightly while solubilize the hydrophobic microdomains (see sections 4.2 and 4.3). In order to investigate the effect of this extra charge on the stability of the samples, DLS measurement were performed on the 1 wt. % nanogels dispersed in 2 mM SDS solution. The resultant hydrodynamic radius and their width of distribution (β) for selection of samples different PEG length are illustrated in Figure 4-12. The graph shows that by adding SDS, R_h for all nanogel systems decreases, and the corresponding width of distribution (β) become narrower at higher temperature. This indicates that even a small amount of SDS (as low as 2mM) can protect particles from aggregation. A comparison between Figure 4-11-a and Figure 4-12 shows an increase in hydrodynamic radius of nanogels in presence SDS at 25°C. This increase is about 17 percent for NG1. Diffusion of SDS into the core and consequent absorption of SDS by PNIPAAm chains is probably responsible for this increase. SDS may decorate PNIPAAm chains with electrostatic charges and prevent them to be packed tightly in the core. This also may suggest that the solubilization is the probable mechanism by which SDS prevents nanogels from aggregation. Hydrodynamic radii for each nanogel dispersed in pure water and in 2 mM SDS solution, at different temperatures are summarized in appendix III.

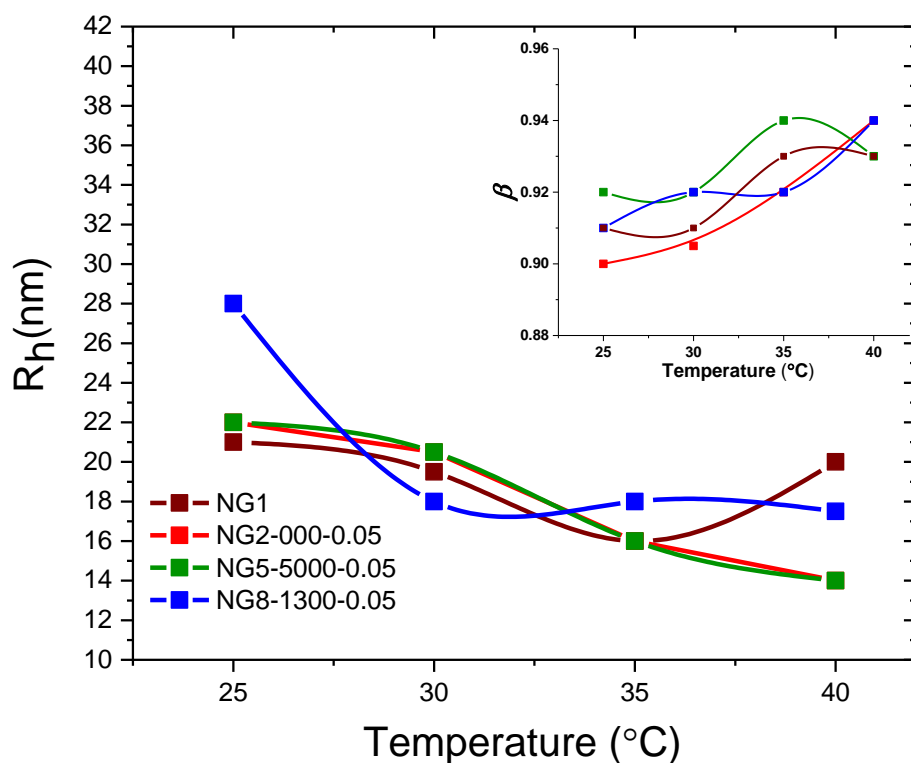


Figure 4-12: Hydrodynamic radii of NG1 (without any PEG layer) and three nanogels coated with different PEG length (2000, 5000 and 13000) vs. temperature in presence of 2mM SDS. The inset plot illustrates the corresponding beta values obtained from DLS. The β values calculated mean values with standard deviation of ± 0.02 .

4.5 Small angle neutron scattering (SANS)

To investigate the influence of temperature on mesoscopic structure of the nanogels, SANS measurements were carried out on 1 wt. % for all samples. The measurements were performed both below and above the CP to study the change in structure of micellar association for different nanogels. In addition, to study the impact of SDS, two selected samples (NG1 and NG2-2000-0.05 with final concentration of 1 wt. %) were measured in 2 mM SDS solution. Figure 4-13 displays the scattering profile as double logarithmic plot of intensity vs. q for all samples at 25 °C. All samples almost overlapped at medium high q , indicating that these samples have the same internal structure. However, by approaching lower q value, curves start to deviate from each other. This suggests some variations on larger scale.

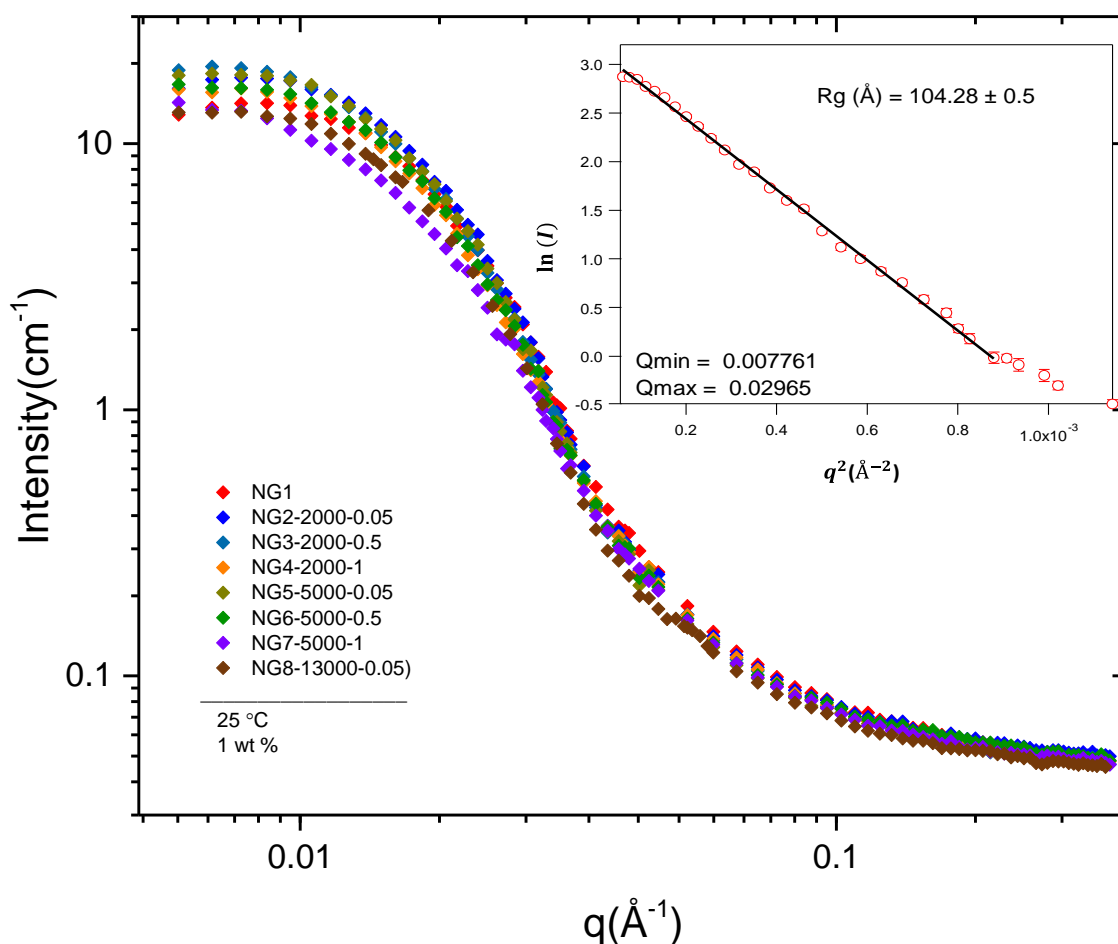


Figure 4-13: SANS scattering profile of 1 wt. % samples in D_2O at 25 °C. The inset plot shows the Guinier fit for NG1 sample.

Table 4-2: Calculated radius of gyrations from Guinier fit and radius of gyration that obtained from model fit.

Sample	Radius of gyration (Å) (at 25°C) fitted via Guinier plot	Radius of gyration (Å) (at 25°C) fitted via SLD	Scattering length (at 25°C) density (10^{-6}Å^{-2})
NG1	98.6 ± 0.5	97 ± 0.1	4.31
NG2-2000-0.05	104.3 ± 0.5	102 ± 0.1	4.29
NG3-2000-0.5	107.8 ± 0.5	107 ± 0.1	4.28
NG4-2000-1	106.0 ± 0.5	---	---
NG5-5000-0.05	106.8 ± 0.5	---	---
NG6-5000-0.5	105.6 ± 0.5	105 ± 0.1	4.43
NG7-5000-1	102.7 ± 0.5	104 ± 0.1	4.80
NG8-13000-0.05	----	106 ± 0.1	4.2

All samples reached a plateau at low q which enabled us to calculate the characteristic size of each system. The inset plot in Figure 4-13 shows the Guinier fit for the NG2-2000-0.05. Guinier fit is a linear fit of log plot of I^{-1} vs. q^2 over low q range (to keep $qR_g < 1$). For some selected samples the R_g values were also calculated with a model fit via scattering length density (SLD) fitting. The obtained R_g and SLD values (at 25°C) are summarized in Table 4-2. It can be observed that the core size of different nanogels at 25° are almost identical (R_g ca. 100 Å), independent from PEG molecular weight. The R_g values obtained from SANS correspond to the core size of nanogels, and the highly hydrated PEG layer is almost undetectable by SANS technique. The almost constant core size of different nanogels indicates that synthesis process was performed in a highly controlled manner.

In order to fit the data several different models were tested, the spherical model can fit the data quite well especially at low q . Figure 4-14 shows SANS scattering profile for NG1 at different temperatures which all were fitted by the spherical model. However a systematic change in scattering density with temperature was observed for NG1. The largest change in scattering intensity was found between 25 and 35 mainly on low q range, indicating increasingly larger particles (i.e. aggregation process). This is likely due to the strong increase in stickiness of PNIPAAm, this effect cannot be fully hindered by the presence of PEG. Other nanogels also displayed the same pattern, for instance the scattering profile for NG3-2000-0.5 and NG6-5000-0.5 in different temperature are illustrated in Figure 4-15-a and b.

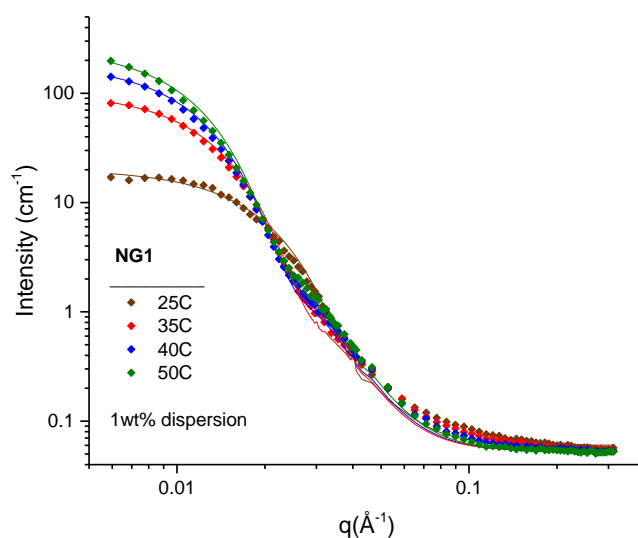


Figure 4-14: SANS scattering profile of 1 wt. % NG1 at different temperatures.

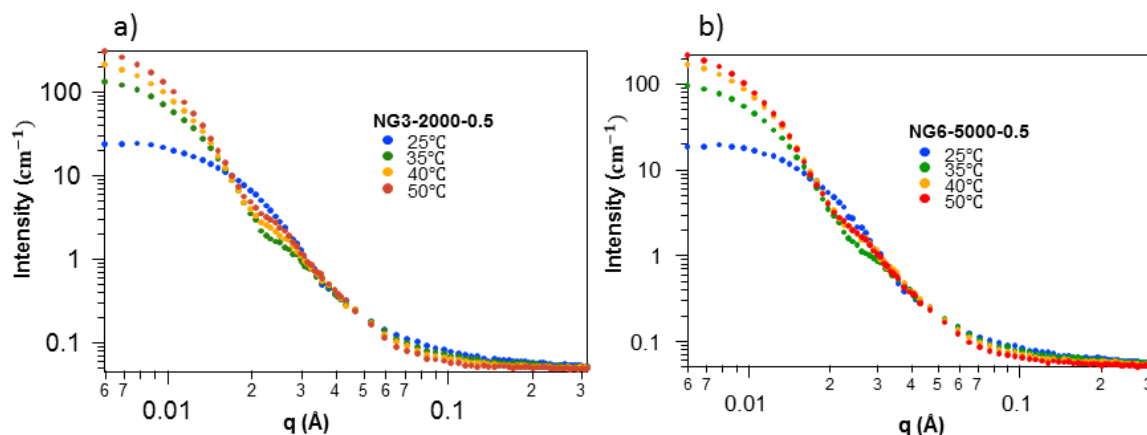


Figure 4-15: SANS scattering profile of 1 wt. % a) NG3-2000-0.5, b) NG6-5000-0.5. Development of “knee” at higher temperature can be observed for both samples.

Figure 4-15-b (left) shows the scattering profile for NG7-5000-1 at different temperatures, and on right hand side the experiments are repeated. It can be seen that the scattering profiles are almost identical, revealing that the aggregation process is fully reversible and the system is highly stable.

The calculated radius of gyration and SLD values at different temperatures for the selected samples are summarized in Table 4-3. The data shows that size of nanogels grows by increasing temperature. However, SANS is not able to “see” the very large particle and these results need to be interpreted in combination with DLS and turbidity, which will be discussed in complementary discussion. On the other hand, the SLD values decline with temperature which is an indication of a more compact core. As the temperature increases the PNIPAAm chains become more hydrophobic and rearrange themselves in a way to have less contact with water, consequently the water will be expelled from the core. This dehydration of the core can also be seen from development of a “knee” around 0.025\AA^{-1} , as seen strongly for e.g. sample NG3-2000-0.5 (see Figure 4-15-a).

In order to study the effect of SDS on stabilization of the nanogels some complementary SANS measurements were performed on NG1 and NG2-2000-0.05. Measurements were done on 1 wt. % of the nanogel dispersion in presence of 2mM SDS. To avoid complications associated with the presence of SDS, deuterated SDS was used in all the experiments. The results from

SANS measurements at all temperatures were fitted by a spherical model and are summarized in Table 4-4. By adding SDS the size of NG1 and NG2-2000-0.05 samples increases about 4 and 6 %, respectively, at 25°C. Comparing Table 4-3 and Table 4-4 shows that the size of the samples without SDS increases with temperature while adding SDS prevents subsequent growth in size. In addition, the SLD values for both samples (NG1 and NG2-2000-0.05) in presence of SDS are higher than SLD values of these nanogels without any SDS at 50°C. This indicates that the core of the nanogels is less contracted in presence of SDS.

Table 4-3: The radius of gyrations for selected 1 wt. % samples in D2O at different temperatures.

Sample	Radius and SLD	25 °C	35 °C	40 °C	50 °C
NG1	R_g (Å)	97	147	167	175
	SLD (10^{-6} \AA^{-2})	4.31	3.88	3.61	3.34
NG2-2000-0.05	R_g (Å)	102	141	160	162
	SLD (10^{-6} \AA^{-2})	4.29	3.75	3.64	3.38
NG3-2000-0.5	R_g (Å)	107	185	203	215
	SLD (10^{-6} \AA^{-2})	4.28	3.91	3.55	3.20
NG6-5000-0.5	R_g (Å)	105	173	190	204
	SLD (10^{-6} \AA^{-2})	4.43	4.15	3.69	3.56
NG7-5000-1	R_g (Å)	104	142	162	179
	SLD (10^{-6} \AA^{-2})	4.80	4.12	3.76	3.57
NG8-13000-1	R_g (Å)	106	138	158	172
	SLD (10^{-6} \AA^{-2})	4.4	4.0	3.7	3.1

Table 4-4: The radius of gyrations for selected 1 wt. % samples in presence of 2mM SDS at different temperatures.

Sample	Radius and SLD	25 °C	35 °C	40 °C	50 °C
NG1	R_g (Å)	101	91	87	97
	SLD (10^{-6} \AA^{-2})	4.5	4.4	4.1	3.8
NG2-2000-0.05	R_g (Å)	108	96	91	99
	SLD (10^{-6} \AA^{-2})	4.5	4.4	4.1	3.8

4.6 *In vitro* cytotoxicity

In order to study the influence of PEG length and concentration on toxicity of synthesized nanogels, a cell viability test was performed on breast cancer cell line in three different nanogels concentrations (5, 15 and 25 $\mu\text{g/ml}$).

Figure 4-16 shows cell viability of nanogels at different concentrations.⁶ The general observation is that by increasing the nanogel concentration toxicity increases, and at 5 $\mu\text{g/ml}$ all nanogels almost showed no sign of toxicity. At higher nanogel concentrations (15 and 25 $\mu\text{g/ml}$) PEG-2000 has almost no effect on increasing cell viability. Viability of PEG-2000 coated nanogels at different concentrations was almost equal to viability of cells treated with nanogels without any PEG coating (NG1). Cell toxicity in the presence of nanogels coated with 0.5 mole % of PEG-5000 decreased compared to nanogels without PEG layer. However, further increase in surface concentration from 0.5 to 1 mole % causes a decrease in cell viability. PEG-5000 with surface concentration of 0.5 mole % is the optimal PEG length and PEG concentration required to achieve the highest cell viability in this study.

Higher toxicity of NG5-5000-1 compared to NG6-5000-0.5 is presumably due to higher polydispersity of NG5-5000-1, which was confirmed by DLS. It has been shown that smaller nanoparticles can induce cell death, while bigger size of the same nanoparticles display low toxicity [73]. β value of NG5-5000-1 obtained from DLS showed that this sample has high

⁶ The NG8-13000-0.05 was not used in macrophage uptake experiments, since it was synthesized just before handing in the thesis.

polydispersity therefore a noticeable fraction of smaller particles may exist. These smaller particles might possibly trigger toxic response.

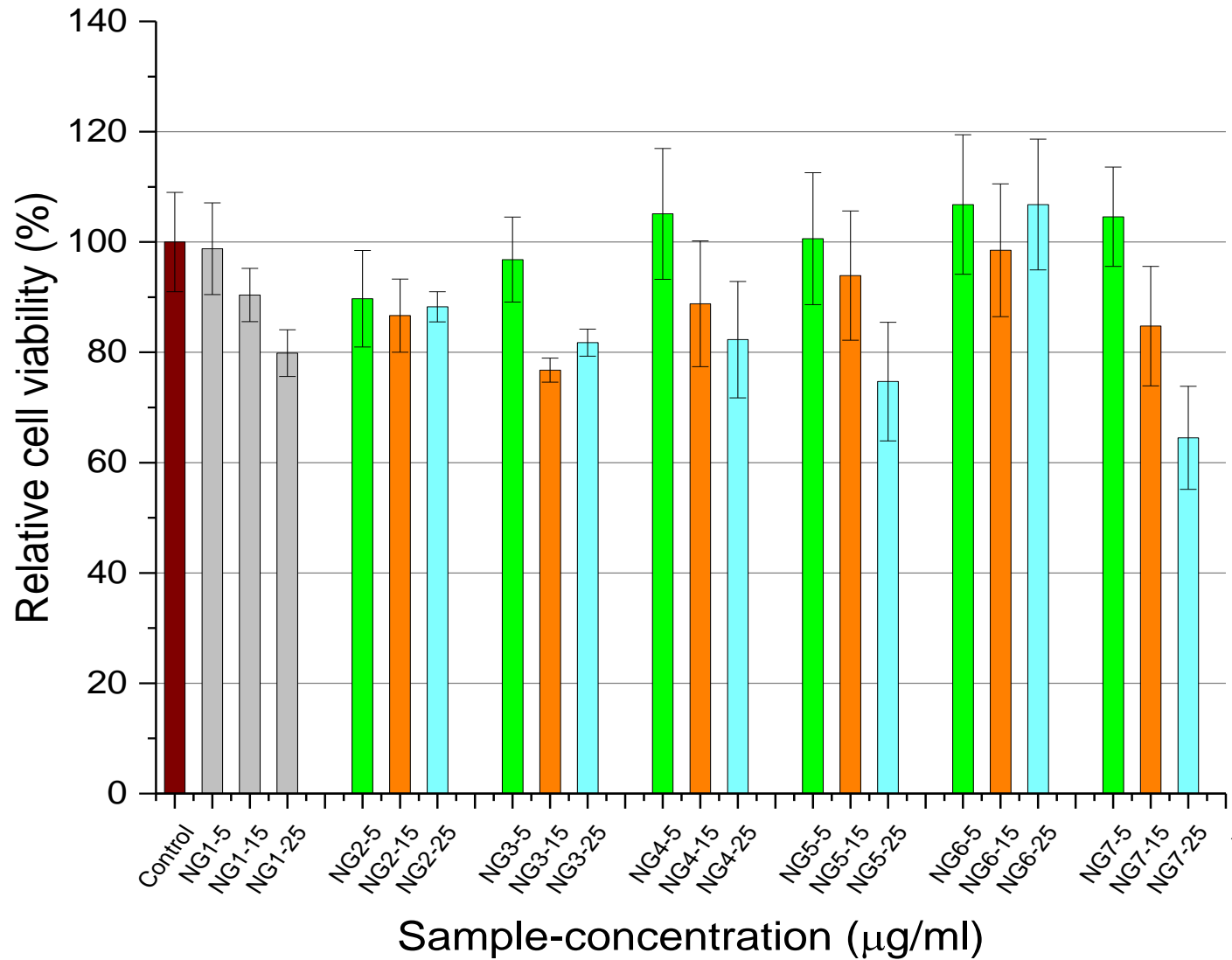


Figure 4-16: Cell viability of seven different nanogels (NG1 to NG7), each samples in three different concentration (5, 15 and 25 $\mu\text{g/ml}$). The brown color is the control and grey colors are the NG1 without PEG layer. For other samples, green, orange and blue colors show the concentration of 5, 15 and 25 $\mu\text{g/ml}$, consecutively. Values are mean \pm SEM (n=4).

4.7 Macrophage uptake

Nanocarriers are usually cleared from the blood stream quickly by immune system and are uptaken by macrophages before they reach to a specific organ in the body. Coating the surface of materials with a layer of PEG molecules showed great promise in overcoming this problem and enables the particle to “hide” from the immune system[74]. To study this effect, uptake of nanogels with different PEG lengths and surface concentrations by THP-1 human acute monocyte cells was studied using confocal microscopy.

Confocal micrographs in Figure 4-17 demonstrate localization of coumarin-6 loaded nanogels (green color) inside the macrophages. Macrophages without any added nanogels were served as control.⁷ The highest macrophage uptake was found for nanogels without any PEG coatings and PEG-2000-0.05. Uptake of nanogels with PEG-5000 at all surface concentrations was lower than uptake of nanogels with PEG-2000 at equivalent surface concentrations. Moreover, by increasing surface concentration of PEG a decrease in macrophage uptake was detected. The most dramatic difference in uptake was observed between surface concentrations of 0.05 and 0.5 mole % for both PEG lengths. The results confirm the significant effect of PEG length and concentration in reducing the uptake of nanogels by macrophages. Considering all stated above, NG6-5000-0.5 has the optimal PEG length and surface concentration for arresting macrophage uptake.

⁷ The NG8-13000-0.05 was not used in macrophage uptake experiments, since it was synthesized just before handing the thesis.

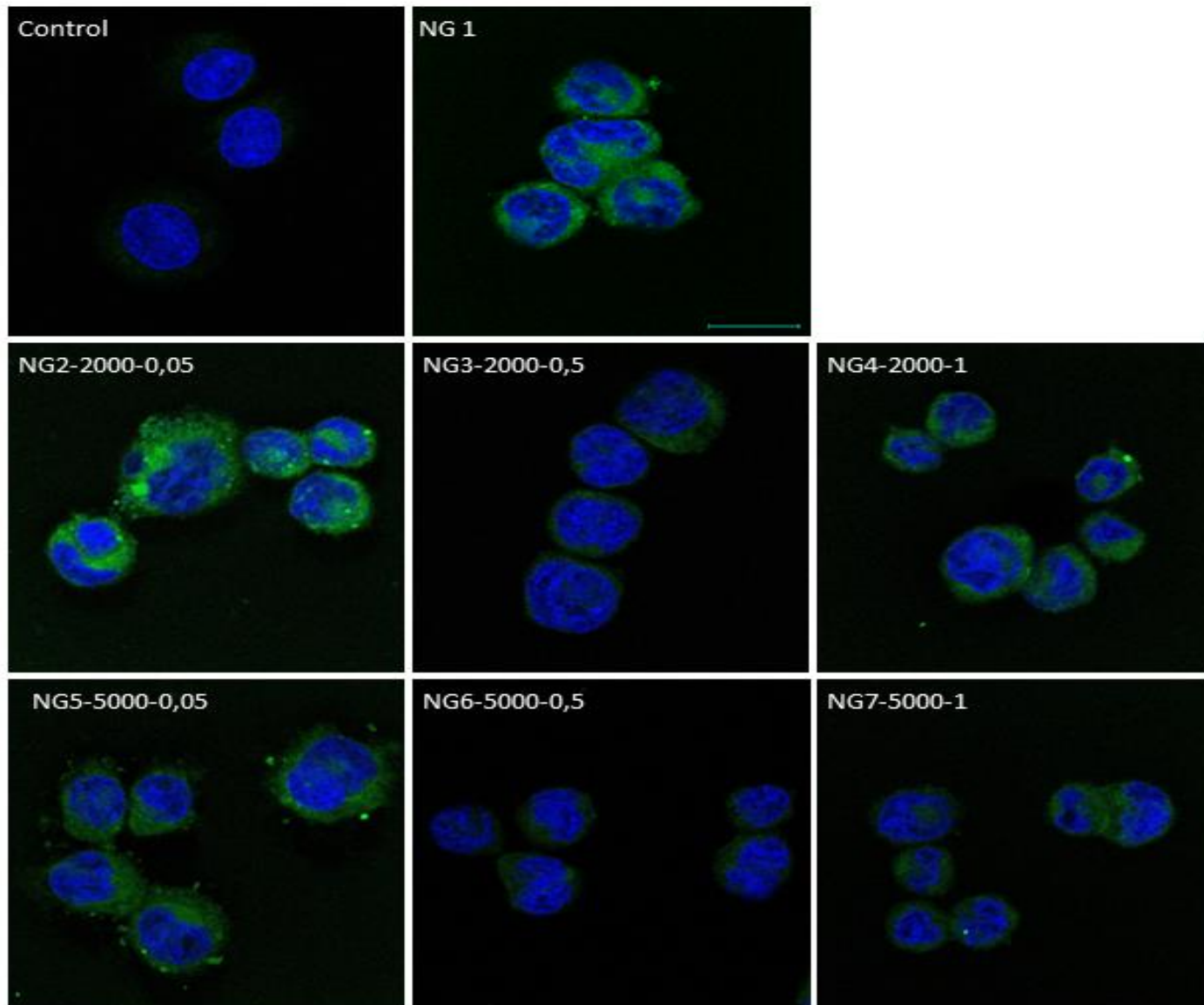


Figure 4-17: Confocal images of uptaken nanogels (green, colored by coumarin-6) by THP-1 human macrophages (macrophages nucleus distinct with blue, colored with DAPI) for seven different nanogels and control sample. The scale bar is the same for all images and it is 20 μm .

4.8 Complementary discussion

The immediate results for each method have been discussed in the previous chapter. In this section some of the results are discussed in a more holistic manner.

The DLS data showed that polydispersity of the samples increases by increasing the mole ratio of PEG. This is due to the fact that above certain wt. % of hydrophilic co-monomer the nucleation process will change. High degree of hydrophilicity prevents the PNIPAAm chains to collapse properly. This results in a more polydisperse system [46].

Turbidity result showed a CP around 28°C for NG1 sample (nanogels without PEG), which is lower than what has previously reported for PNIPAAm (32°C) [71]. This probably is due to the presence of methacrylic acid and BAC which make nanogels more hydrophobic than PNIPAAm itself.

The radius values obtained from SANS experiments are not the same as hydrodynamic radius calculated from DLS measurements. This discrepancy can have can be explained by the fact that SANS technique mainly detects the core when the shell is highly hydrated. Therefore, the structural size found from SANS is usually smaller than the hydrodynamic size (R_h) found from DLS.

By dividing R_g and R_h values obtained from SANS and DLS respectively, the shape of nanogels can be predicted. The R_g/R_h ratio for NG1 was around 0.6, by increasing PEG content (NG7-5000-1 and NG8-13000-0.05) this ratio drops below 0.5. The ratio around 0.6 suggests a uniform solid sphere for these systems. This structure was also confirmed by the SANS model fit. R_g/R_h ratio for high PEG content samples was below 0.5 which cannot give any information about the structure of these systems and has not been reported. The ratios below 0.5 may indicate that PEG chains are “invisible” in SANS technique, while DLS can detect them.

By increasing the temperature, R_g values calculated from SANS experiments increases continuously. The size also increased with temperature as measured by DLS except for the nanogel with the highest PEG length (PEG-13000). This increase in size is observed by SANS and

DLS in addition to the turbidity measurement results, and suggest that aggregation happens at higher temperature except for the nanogel with the highest PEG length (PEG-13000). The size of the nanogels with PEG-13000 decreased slightly in DLS. The decrease in turbidity signal for nanogels with PEG-13000 layer at higher temperature also confirms aggregation did not happen for this nanogel. This result is suggesting the PEG-13000 is minimum needed length for stabilization of our system.

The increase in R_g values of the nanogel with PEG-13000 with temperature despite the slight decrease of R_h values can be explained by collapsing of PEG-13000 chains on to the surface of nanogels core. It is possible that the increased segment density of the PEG chains around the core made the PEG chains detectable by SANS.

5 Conclusion

In this study we investigated the effect of PEG length and PEG surface density on stabilization of PNIPAAm-co-MAA nanogels by preparing eight different nanogels with various PEG lengths and PEG surface concentration. The influence of electrostatic charge in stabilization of nanogels was also studied by adding SDS.

The general observation is that by increasing the temperature, the size of the nanogels increase as well and the systems tend to form aggregates. However, by adding a small amount of SDS, the aggregation process is suppressed significantly as measured by turbidity, DLS and SANS techniques.

By increasing the PEG surface concentration of different nanogels systems the CP shifted towards higher temperatures, which shows that increasing PEG concentration can arrest aggregation to some extent. However, when the PEG chains with insufficient length are used, increasing PEG concentration cannot completely prevent aggregation and leads to forming more polydisperse systems.

Preparing nanogels with different PEG lengths showed that PEG length definitely has an effect in preventing aggregation. In this study a minimum PEG length of 13000 was required to prevent these systems from forming aggregates. Nanogels with PEG-13000 showed this effect even at the lowest surface concentration.

The number of viable cells in presence of PEG-2000 nanogels was almost the same as nanogels without any PEG, showing that decorating the surface of nanogels with PEG-2000 does not contribute to increasing viability of the cells. However, by increasing the PEG length to 5000 the cell viability increases. Further increase of surface concentration of PEG-5000 led to drastic decrease in cell viability.

The same trend was observed in the macrophage uptake experiment. The nanogels provided with 0.5 mole percent of PEG-5000 showed the least macrophage uptake. This observation confirms the effect of increasing hydrophilicity in lowering probability of the

nanogels to be considered as foreign object in cell environment.

5.1 Future work

PEG oligomers can have different structures. Different structures of can provide unique properties (e.g. surface area, size and effective length) for biological experiment and steric stabilization of nanoparticles [75]. PEG oligomers utilized in this study had a linear structure. For future studies I propose utilization of branched PEG oligomers with equivalent molecular weights as the linear PEG oligomers used in this study. It will be interesting to compare biological activity and steric stability of branched PEG oligomers with linear PEG oligomers. Furthermore, conjugating other highly hydrophilic polymers such as dextran to the surface of the nanogels with the same molecular weight as PEG oligomers would be a matter of interest.

Bibliography

1. van Rijt, S.H., Bein, T., and Meiners, S., *Medical nanoparticles for next generation drug delivery to the lungs*. European Respiratory Journal, 2014. **44**(3): p. 765-774.
2. Mosqueira, V.C.F., Legrand, P., Gulik, A., Bourdon, O., Gref, R., Labarre, D., and Barratt, G., *Relationship between complement activation, cellular uptake and surface physicochemical aspects of novel PEG-modified nanocapsules*. Biomaterials, 2001. **22**(22): p. 2967-2979.
3. Williams, A.E., *Immunology: mucosal and body surface defences*. 2011: John Wiley & Sons.
4. Sheng, Y., Yuan, Y., Liu, C., Tao, X., Shan, X., and Xu, F., *In vitro macrophage uptake and in vivo biodistribution of PLA-PEG nanoparticles loaded with hemoglobin as blood substitutes: effect of PEG content*. Journal of Materials Science: Materials in Medicine, 2009. **20**(9): p. 1881-1891.
5. Zahr, A.S., Davis, C.A., and Pishko, M.V., *Macrophage uptake of core-shell nanoparticles surface modified with poly (ethylene glycol)*. Langmuir, 2006. **22**(19): p. 8178-8185.
6. Mosqueira, V., Legrand, P., Gref, R., Heurtault, B., Appel, M., and Barratt, G., *Interactions between a macrophage cell line (J774A1) and surface-modified poly (D, L-lactide) nanocapsules bearing poly (ethylene glycol)*. Journal of Drug Targeting, 1999. **7**(1): p. 65-78.
7. Nel, A., Xia, T., Mädler, L., and Li, N., *Toxic potential of materials at the nanolevel*. Science, 2006. **311**(5761): p. 622-627.
8. Moore, T.L., Rodriguez-Lorenzo, L., Hirsch, V., Balog, S., Urban, D., Jud, C., Rothen-Rutishauser, B., Lattuada, M., and Petri-Fink, A., *Nanoparticle colloidal stability in cell culture media and impact on cellular interactions*. Chemical Society Reviews, 2015. **44**(17): p. 6287-305.
9. Abuchowski, A., McCoy, J.R., Palczuk, N.C., van Es, T., and Davis, F.F., *Effect of covalent attachment of polyethylene glycol on immunogenicity and circulating life of bovine liver catalase*. Journal of Biological Chemistry, 1977. **252**(11): p. 3582-3586.
10. Abuchowski, A., Van Es, T., Palczuk, N., and Davis, F., *Alteration of immunological properties of bovine serum albumin by covalent attachment of polyethylene glycol*. Journal of Biological Chemistry, 1977. **252**(11): p. 3578-3581.
11. Harris, J.M., Martin, N.E., and Modi, M., *Pegylation*. Clinical Pharmacokinetics, 2001. **40**(7): p. 539-551.
12. Veronese, F.M. and Mero, A., *The Impact of PEGylation on Biological Therapies*. BioDrugs, 2008. **22**(5): p. 315-329.
13. Kenworthy, A.K., Hristova, K., Needham, D., and McIntosh, T.J., *Range and magnitude of the steric pressure between bilayers containing phospholipids with covalently attached poly (ethylene glycol)*. Biophysical Journal, 1995. **68**(5): p. 1921-1936.

14. Suk, J.S., Xu, Q., Kim, N., Hanes, J., and Ensign, L.M., *PEGylation as a strategy for improving nanoparticle-based drug and gene delivery*. *Advanced Drug Delivery Reviews*, 2016. **99**: p. 28-51.
15. Kumari, A., Yadav, S.K., and Yadav, S.C., *Biodegradable polymeric nanoparticles based drug delivery systems*. *Colloids and Surfaces B: Biointerfaces*, 2010. **75**(1): p. 1-18.
16. Ruoslahti, E., Bhatia, S.N., and Sailor, M.J., *Targeting of drugs and nanoparticles to tumors*. *Journal of Cell Biology*, 2010. **188**(6): p. 759-68.
17. Cho, K., Wang, X., Nie, S., and Shin, D.M., *Therapeutic nanoparticles for drug delivery in cancer*. *Clinical Cancer Research*, 2008. **14**(5): p. 1310-1316.
18. Klinger, D. and Landfester, K., *Stimuli-responsive microgels for the loading and release of functional compounds: Fundamental concepts and applications*. *Polymer*, 2012. **53**(23): p. 5209-5231.
19. Letchford, K. and Burt, H., *A review of the formation and classification of amphiphilic block copolymer nanoparticulate structures: micelles, nanospheres, nanocapsules and polymersomes*. *European Journal of Pharmaceutics and Biopharmaceutics*, 2007. **65**(3): p. 259-269.
20. Mishra, D., Hubenak, J.R., and Mathur, A.B., *Nanoparticle systems as tools to improve drug delivery and therapeutic efficacy*. *Journal of Biomedical Materials Research*, 2013. **101**(12): p. 3646-60.
21. Qiao, W., Wang, B., Wang, Y., Yang, L., Zhang, Y., and Shao, P., *Cancer Therapy Based on Nanomaterials and Nanocarrier Systems*. *Journal of Nanomaterials*, 2010. **2010**: p. 1-9.
22. Lee, C.C., MacKay, J.A., Frechet, J.M., and Szoka, F.C., *Designing dendrimers for biological applications*. *Nature Biotechnology*, 2005. **23**(12): p. 1517-26.
23. Wang, H., Huang, Q., Chang, H., Xiao, J., and Cheng, Y., *Stimuli-responsive dendrimers in drug delivery*. *Biomaterials science*, 2016. **4**(3): p. 375-90.
24. Tomalia, D., Baker, H., Dewald, J., Hall, M., Kallos, G., Martin, S., Roeck, J., Ryder, J., and Smith, P., *A New Class of Polymers: Starburst-Dendritic*. *Polymer Journal*, 1985. **17**(1): p. 117-132.
25. Rastogi, R., Anand, S., and Koul, V., *Flexible polymerosomes--an alternative vehicle for topical delivery*. *Colloids and Surfaces B: Biointerfaces*, 2009. **72**(1): p. 161-6.
26. Discher, D.E. and Eisenberg, A., *Polymer vesicles*. *Science*, 2002. **297**(5583): p. 967-973.
27. Tanner, P., Baumann, P., Enea, R., Onaca, O., Palivan, C., and Meier, W., *Polymeric vesicles: from drug carriers to nanoreactors and artificial organelles*. *Accounts of Chemical Research*, 2011. **44**(10): p. 1039-1049.
28. Li, M.-H. and Keller, P., *Stimuli-responsive polymer vesicles*. *Soft Matter*, 2009. **5**(5): p. 927-937.

29. Mark, J.E., *Physical properties of polymers handbook*. Vol. 1076. 2007: Springer.
30. Das, M., Zhang, H., and Kumacheva, E., *Microgels: old materials with new applications*. Annual Review of Materials Research, 2006. **36**: p. 117-142.
31. Staudinger, H. and Husemann, E., *Über hochpolymere Verbindungen, 118. Mitteil.: Viscositäts - Untersuchungen an organischen Sphäro - und Linear - kolloiden*. Berichte der deutschen chemischen Gesellschaft, 1935. **68**(9): p. 1691-1697.
32. Mason, W., Baker, W., McSkimin, H., and Heiss, J., *Measurement of shear elasticity and viscosity of liquids at ultrasonic frequencies*. Physical Review, 1949. **75**(6): p. 936-946.
33. Pelton, R. and Hoare, T., *Microgels and their synthesis: An introduction*. Microgel Suspensions: Fundamentals and Applications, 2011. **1**: p. 1-32.
34. Zha, L., Banik, B., and Alexis, F., *Stimulus responsive nanogels for drug delivery*. Soft Matter, 2011. **7**(13): p. 5908-5916.
35. Jiang, Y., Chen, J., Deng, C., Suuronen, E.J., and Zhong, Z., *Click hydrogels, microgels and nanogels: emerging platforms for drug delivery and tissue engineering*. Biomaterials, 2014. **35**(18): p. 4969-4985.
36. Vinogradov, S.V., Bronich, T.K., and Kabanov, A.V., *Nanosized cationic hydrogels for drug delivery: preparation, properties and interactions with cells*. Advanced Drug Delivery Reviews, 2002. **54**(1): p. 135-147.
37. Everett, D.H., *Basic principles of colloid science*. 1988: Royal Society of Chemistry.
38. Block, L.P., *A double layer review*. Astrophysics and Space Science, 1978. **55**(1): p. 59-83.
39. Polte, J., *Fundamental growth principles of colloidal metal nanoparticles—a new perspective*. CrystEngComm, 2015. **17**(36): p. 6809-6830.
40. Derjaguin, B. and Landau, L., *The theory of stability of highly charged lyophobic sols and coalescence of highly charged particles in electrolyte solutions*. Acta Physicochim. URSS, 1941. **14**(633-52): p. 58.
41. Hermansson, M., *The DLVO theory in microbial adhesion*. Colloids and Surfaces B: Biointerfaces, 1999. **14**(1): p. 105-119.
42. Griffin, J.M., Robb, I., and Bismarck, A., *Preparation and characterization of surfactant - free stimuli - sensitive microgel dispersions*. Journal of Applied Polymer Science, 2007. **104**(3): p. 1912-1919.
43. Miao, C., Chen, X., and Pelton, R., *Adhesion of poly (vinylamine) microgels to wet cellulose*. Industrial & Engineering Chemistry Research, 2007. **46**(20): p. 6486-6493.
44. Sivakumaran, D., Mueller, E., and Hoare, T., *Temperature-induced assembly of monodisperse, covalently cross-linked, and degradable poly (N-isopropylacrylamide) microgels based on oligomeric precursors*. Langmuir, 2015. **31**(21): p. 5767-5778.

45. Saunders, B.R. and Vincent, B., *Microgel particles as model colloids: theory, properties and applications*. Advances in Colloid and Interface Science, 1999. **80**(1): p. 1-25.
46. Nayak, S. and Lyon, L.A., *Soft nanotechnology with soft nanoparticles*. Angewandte Chemie International Edition, 2005. **44**(47): p. 7686-7708.
47. Bonham, J.A., Faers, M.A., and van Duijneveldt, J.S., *Non-aqueous microgel particles: synthesis, properties and applications*. Soft Matter, 2014. **10**(47): p. 9384-98.
48. Ward, M.A. and Georgiou, T.K., *Thermoresponsive polymers for biomedical applications*. Polymers, 2011. **3**(3): p. 1215-1242.
49. Eeckman, F., Moës, A.J., and Amighi, K., *Evaluation of a new controlled-drug delivery concept based on the use of thermoresponsive polymers*. International Journal of Pharmaceutics, 2002. **241**(1): p. 113-125.
50. Heskins, M. and Guillet, J.E., *Solution properties of poly (N-isopropylacrylamide)*. Journal of Macromolecular Science—Chemistry, 1968. **2**(8): p. 1441-1455.
51. Roy, D., Brooks, W.L., and Sumerlin, B.S., *New directions in thermoresponsive polymers*. Chemical Society Reviews, 2013. **42**(17): p. 7214-7243.
52. Hashemi, M. and Chasteen, T.G., *Hofmeister effect challenge*. Analytical and Bioanalytical Chemistry, 2011. **400**(3): p. 643-644.
53. Fanaian, S., Al-Manasir, N., Zhu, K., Kjøniksen, A.-L., and Nyström, B., *Effects of Hofmeister anions on the flocculation behavior of temperature-responsive poly (N-isopropylacrylamide) microgels*. Colloid and Polymer Science, 2012. **290**(16): p. 1609-1616.
54. Chu, B., *Dynamic Light Scattering*, in *Soft Matter Characterization*. 2008, Springer Netherlands: Dordrecht. p. 335-372.
55. Pecora, R., *Basic Concepts – Scattering and Time Correlation Functions*, in *Soft Matter Characterization*. 2008, Springer Netherlands: Dordrecht. p. 2-40.
56. Siegert, A., *On the fluctuations in signals returned by many independently moving scatterers*. 1943: Radiation Laboratory, Massachusetts Institute of Technology.
57. Kjøniksen, A.-L., Zhu, K., Behrens, M.A., Pedersen, J.S., and Nyström, B., *Effects of temperature and salt concentration on the structural and dynamical features in aqueous solutions of charged triblock copolymers*. The Journal of Physical Chemistry B, 2011. **115**(10): p. 2125-2139.
58. Bhattacharjee, S., *DLS and zeta potential – What they are and what they are not?* Journal of Controlled Release, 2016. **235**: p. 337-351.
59. Honary, S. and Zahir, F., *Effect of zeta potential on the properties of nano-drug delivery systems-a review (Part 1)*. Tropical Journal of Pharmaceutical Research, 2013. **12**(2): p. 255-264.

60. Clogston, J.D. and Patri, A.K., *Zeta potential measurement*. Characterization of nanoparticles intended for drug delivery, 2011: p. 63-70.
61. Kjøniksen, A.-L., Laukkanen, A., Galant, C., Knudsen, K.D., Tenhu, H., and Nyström, B., *Association in aqueous solutions of a thermoresponsive PVCL-g-C11EO42 copolymer*. *Macromolecules*, 2005. **38**(3): p. 948-960.
62. Penfold, J. and Thomas, R.K., *Neutron reflectivity and small angle neutron scattering: An introduction and perspective on recent progress*. *Current Opinion in Colloid & Interface Science*, 2014. **19**(3): p. 198-206.
63. Gosecka, M. and Gosecki, M., *Characterization methods of polymer core-shell particles*. *Colloid and Polymer Science*, 2015. **293**(10): p. 2719-2740.
64. Pedersen, J.S., Svaneborg, C., Almdal, K., Hamley, I.W., and Young, R.N., *A small-angle neutron and X-ray contrast variation scattering study of the structure of block copolymer micelles: corona shape and excluded volume interactions*. *Macromolecules*, 2003. **36**(2): p. 416-433.
65. Ermi, B.D. and Amis, E.J., *Domain structures in low ionic strength polyelectrolyte solutions*. *Macromolecules*, 1998. **31**(21): p. 7378-7384.
66. Schanda, P. and Ernst, M., *Studying dynamics by magic-angle spinning solid-state NMR spectroscopy: Principles and applications to biomolecules*. *Progress in Nuclear Magnetic Resonance Spectroscopy*, 2016. **96**: p. 1-46.
67. Claridge, T.D., *High-resolution NMR techniques in organic chemistry*. Vol. 27. 2016: Elsevier.
68. Hore, P.J., *Nuclear magnetic resonance*. Oxford chemistry primers. Vol. 32. 1995, Oxford: Oxford University Press.
69. Jones, J.A., Novo, N., Flagler, K., Pagnucco, C.D., Carew, S., Cheong, C., Kong, X.Z., Burke, N.A., and Stöver, H.D., *Thermoresponsive copolymers of methacrylic acid and poly (ethylene glycol) methyl ether methacrylate*. *Journal of Polymer Science Part A: Polymer Chemistry*, 2005. **43**(23): p. 6095-6104.
70. Deshmukh, M., Vaidya, A., Kulkarni, M., Rajamohanam, P., and Ganapathy, S., *LCST in poly (N-isopropylacrylamide) copolymers: high resolution proton NMR investigations*. *Polymer*, 2000. **41**(22): p. 7951-7960.
71. Pamies, R., Zhu, K., Kjøniksen, A.-L., and Nyström, B., *Thermal response of low molecular weight poly-(N-isopropylacrylamide) polymers in aqueous solution*. *Polymer Bulletin*, 2009. **62**(4): p. 487-502.
72. Pamies, R., Zhu, K., Kjøniksen, A.-L., Knudsen, K.D., and Nyström, B., *Temperature-induced intermicellization and contraction in aqueous mixtures of sodium dodecyl sulfate and an amphiphilic diblock copolymer*. *Journal of Colloid and Interface Science*, 2008. **326**(1): p. 76-88.
73. Pan, Y., Neuss, S., Leifert, A., Fischler, M., Wen, F., Simon, U., Schmid, G., Brandau, W., and

- Jahnen - Dechent, W., *Size - dependent cytotoxicity of gold nanoparticles*. *Small*, 2007. **3**(11): p. 1941-1949.
74. Bazile, D., Prud'homme, C., Bassoullet, M.T., Marlard, M., Spenlehauer, G., and Veillard, M., *Stealth Me. PEG - PLA nanoparticles avoid uptake by the mononuclear phagocytes system*. *Journal of Pharmaceutical Sciences*, 1995. **84**(4): p. 493-498.
75. Veronese, F.M., Caliceti, P., and Schiavon, O., *Branched and linear poly(ethylene glycol): Influence of the polymer structure on enzymological, pharmacokinetic, and immunological properties of protein conjugates*. *Journal of Bioactive and Compatible Polymers*, 1997. **12**(3): p. 196-207.

Appendix

Appendix I: NMR results

The NMR data are shown in figures below. Two peak “b” and “i” are selected to calculate the final mole percent of PEG, assuming all other monomers are consumed completely. Peak “b” is assigned to one NIPAM hydrogen and peak “i” is caused by four PEG hydrogens. The Number of repeating unit for each PEG was calculated from their Mn. Mn was calculated from below equation $PDI = M_w/M_n$ (M_w and PDI of PEG was provided by the manufacturer). The mole percent of PEG was calculated as follows:

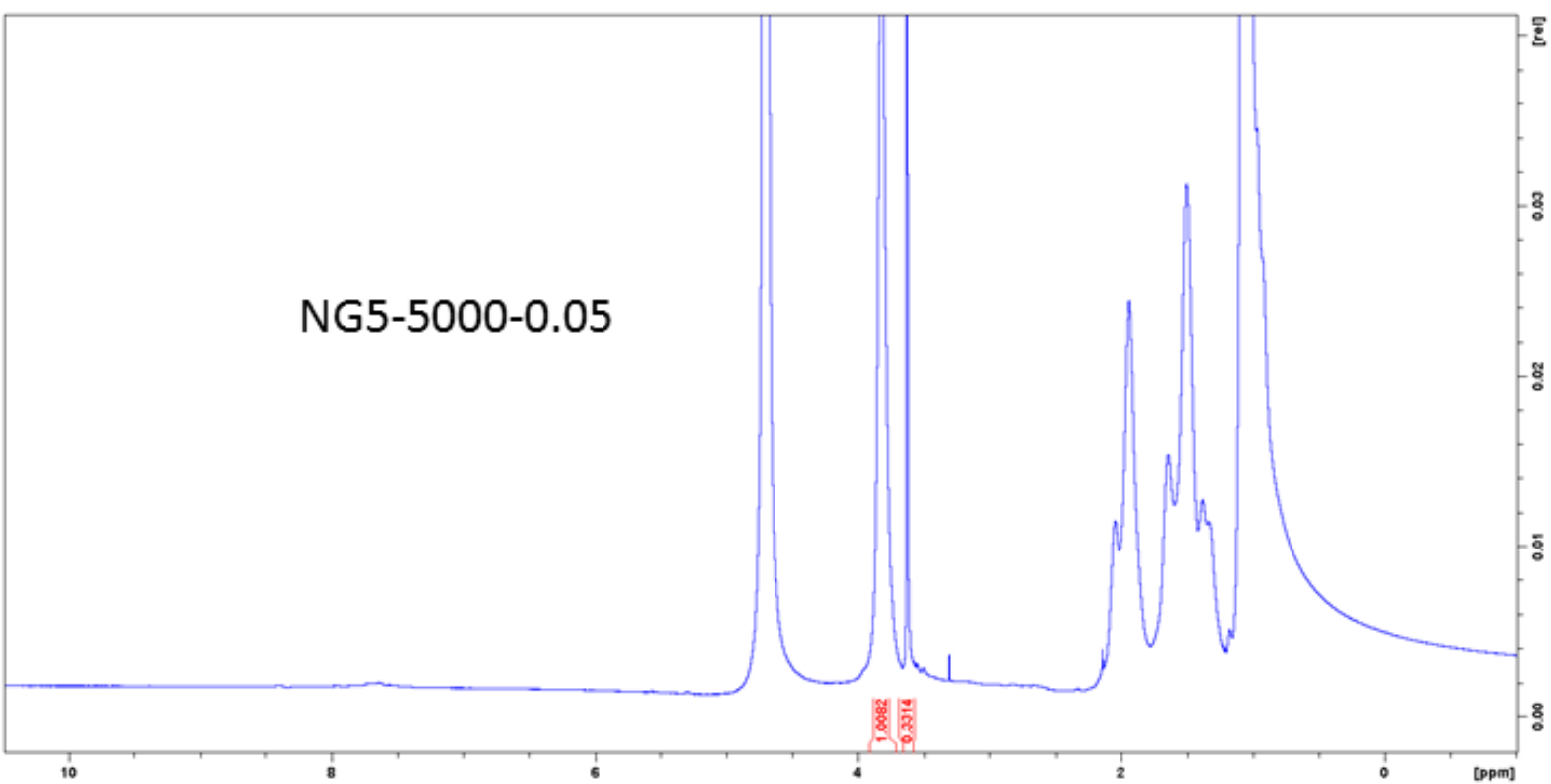
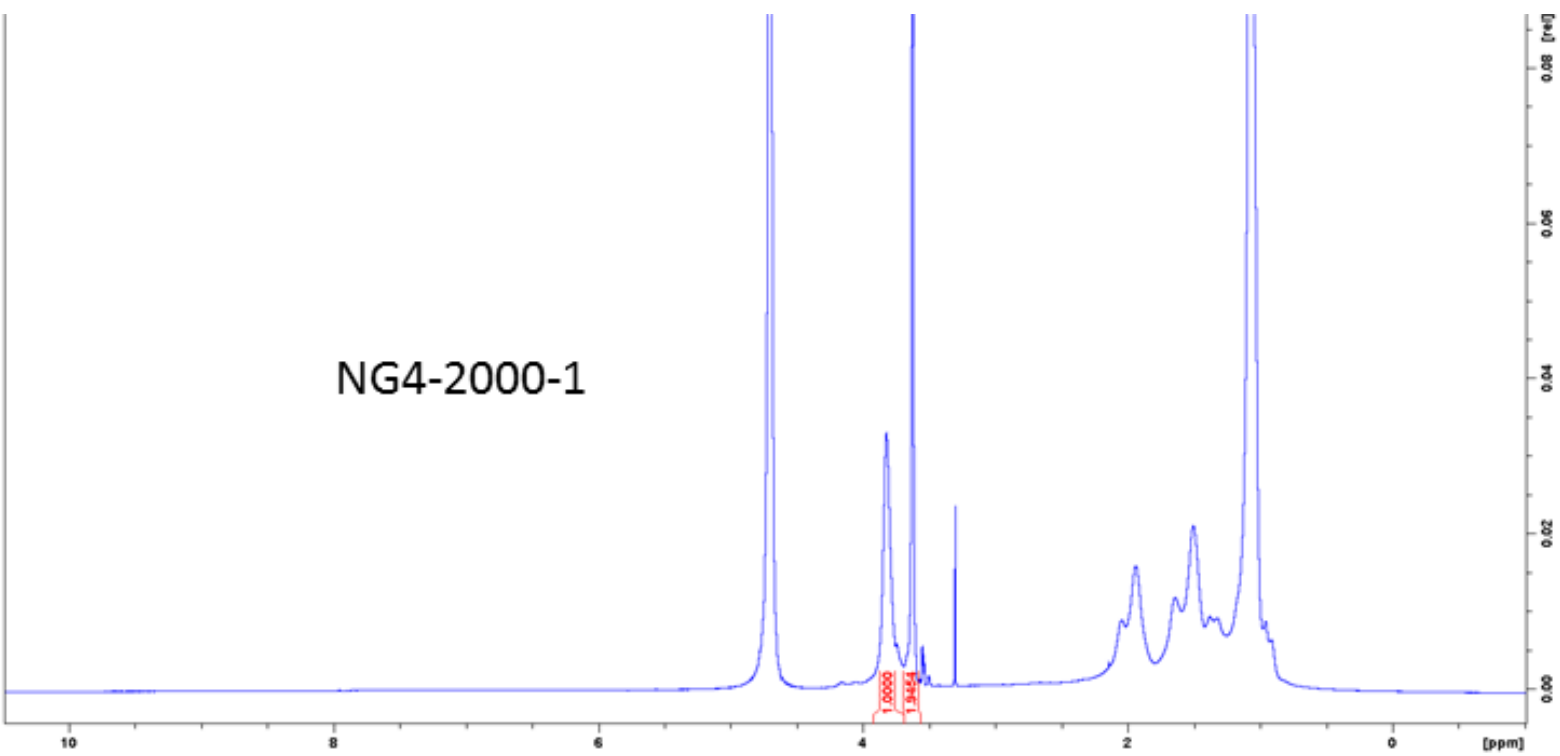
The initial ratio (mole % of compound added to the reactor) of the two peaks can be determined by the following equation:

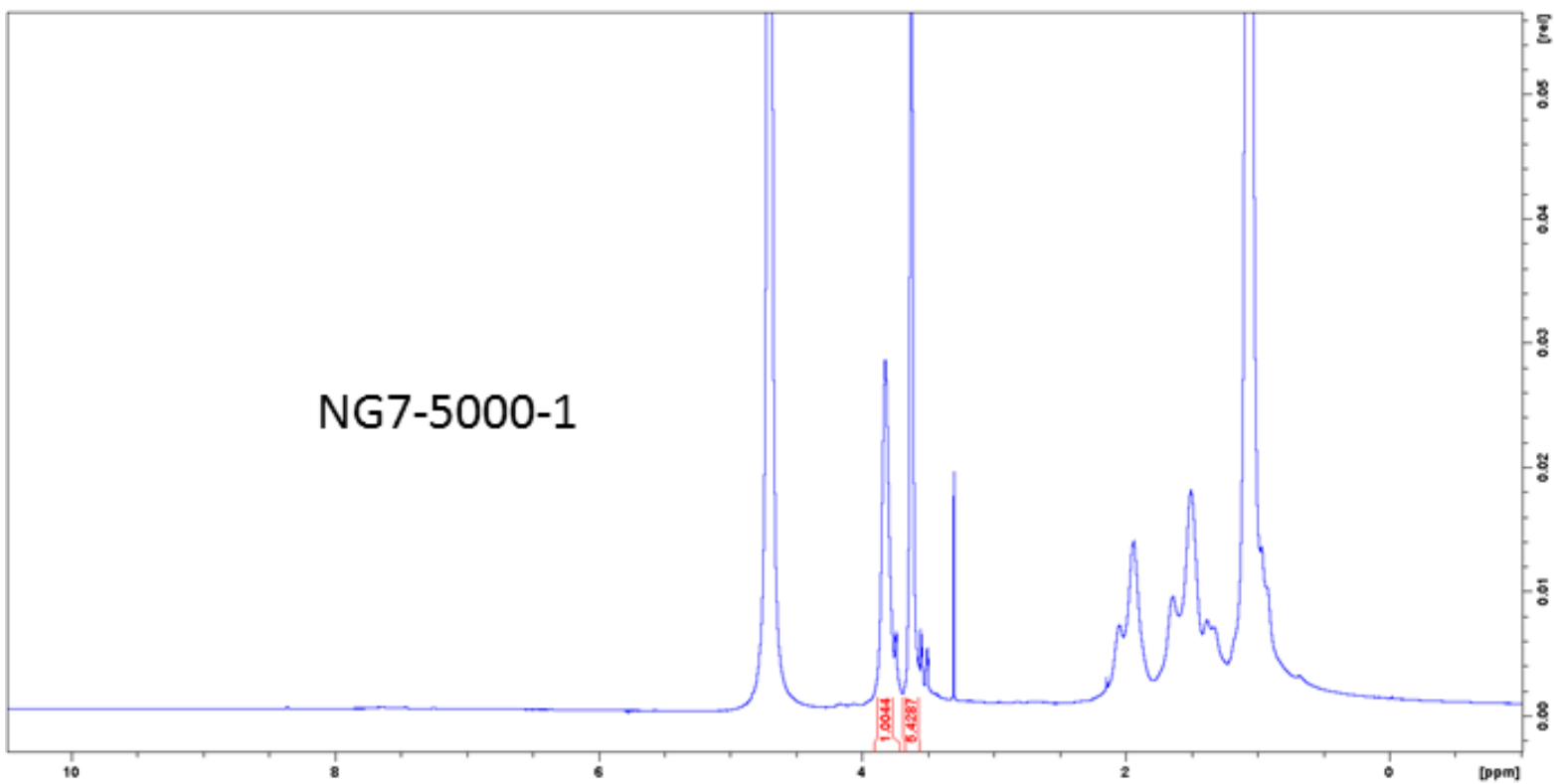
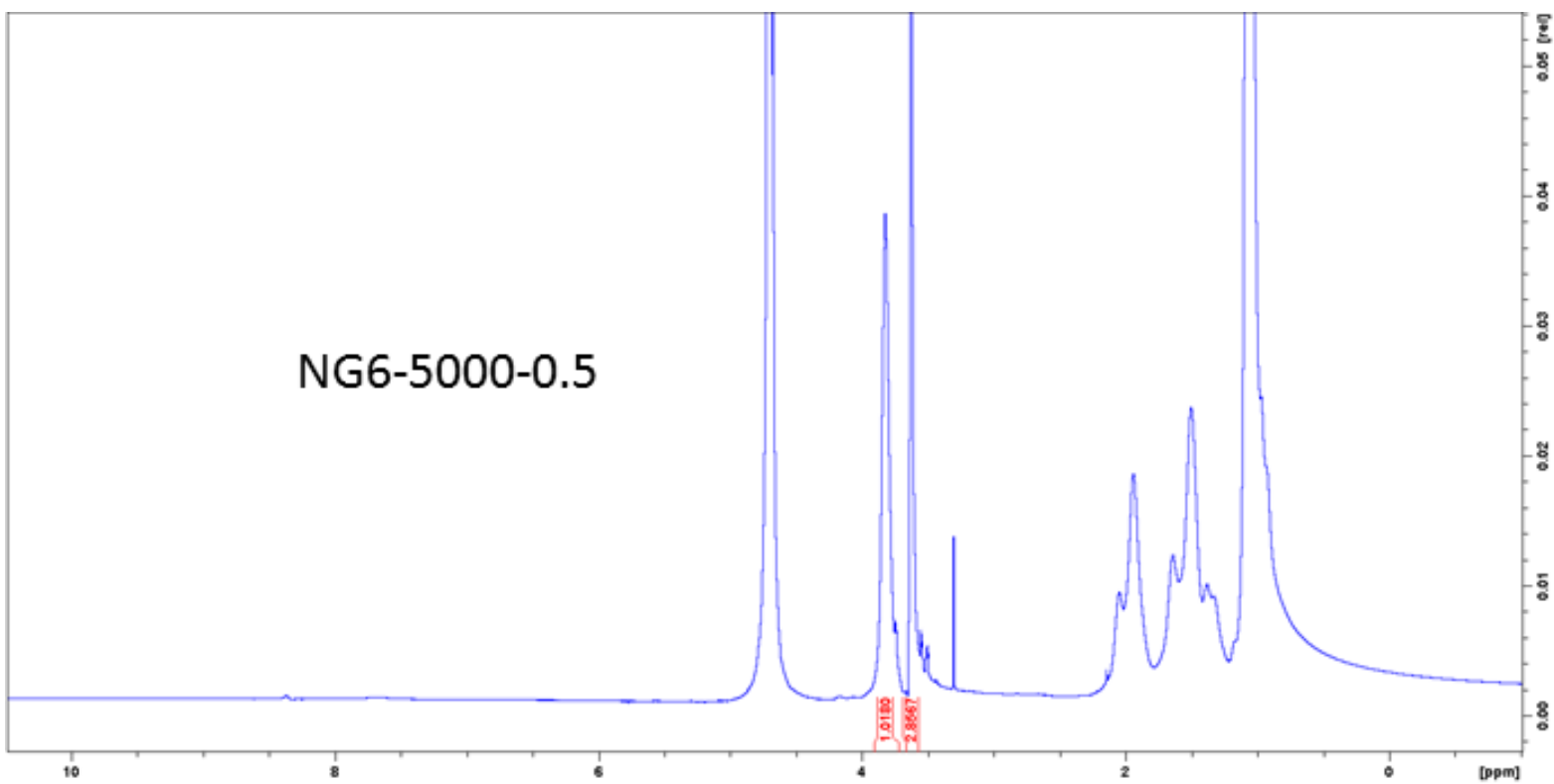
$$\text{Initial ratio} = \frac{\text{mole percent of NIPAM} \times 1}{\text{mole percent of PEG} \times \text{number of repeating units} \times 4}$$

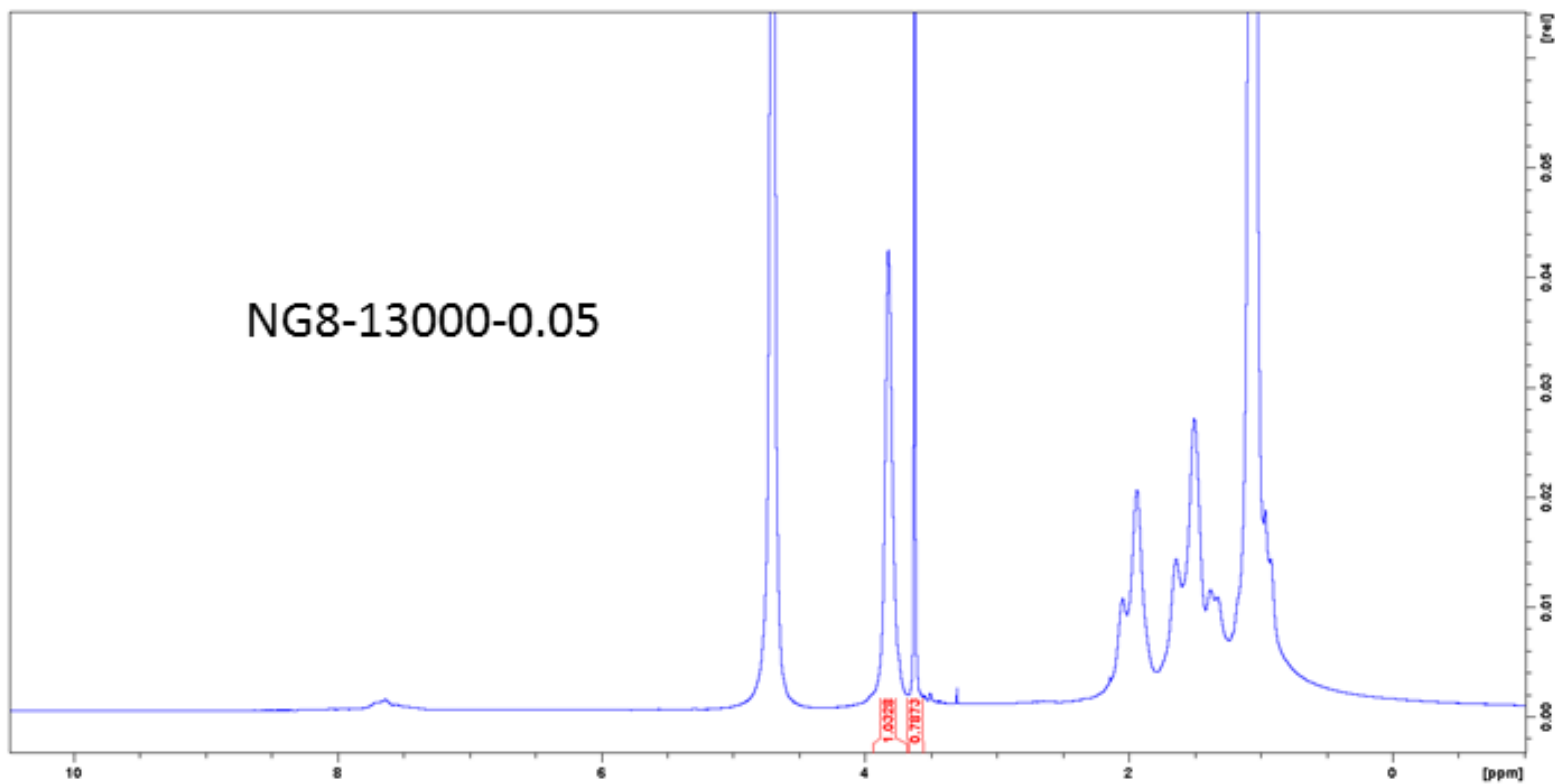
The resultant ratio after dialysis can easily be obtained from NMR (by dividing the integrated number). The resultant mole percent of PEG can be calculated from below equation (assuming all other monomers consumed completely).

$$\text{resultant mole \% PEG} = \frac{\text{initial ratio}}{\text{resultant ratio}} \times \text{initial mole percent of PEG}$$

The NMR spectrums for all samples are shown in following figures.







Appendix II: Turbidity measurements

The cloud points (CP) for all nanogels in different conditions are summarized in the table below.

Sample \ Condition	1 wt. % water	2.5 wt. % water	1 wt. % 0.01M NaCl	1 wt. % 0.05M NaCl	1 wt. % 0.1M NaCl
NG1	28.5	27.5	28	28	27.5
NG2-(2000/0.05)	29	28	28.5	28.5	28
NG3-(2000/0.5)	31.5	28.5	28	28	28.5
NG4-(2000/1)	36	29	30.5	29.5	29
NG5-(5000/0.05)	29.5	30	30.5	29.5	28.5
NG6-(5000/0.5)	37.5	32	30	29.5	28.5
NG7-(5000/1)	39	38	32	30	29
NG8-(13000/0.05)	---	34	34	31.5	29.5

Appendix III: Hydrodynamic radii for all samples in water and 2 mM SDS solution

The hydrodynamic radii which are obtained by DLS, for all nanogels in pure water medium and in presence of 2 mM SDS are summarized in below table.

sample	Radius-Medium	25°C	30°C	35°C	40°C
NG1	R_h (nm)-pure water	17	34	51	73
NG1	R_h (nm)-2 mM SDS	21	19.5	16	20
NG2-2000-0.05	R_h (nm)-pure water	19	23	44	52
NG2-2000-0.05	R_h (nm)-2 mM SDS	22	20.5	16	14
NG3-2000-0.5	R_h (nm)-pure water	21	38	34	34
NG3-2000-0.5	R_h (nm)-2 mM SDS	22.5	21	19	18
NG4-2000-1	R_h (nm)-pure water	23	40	36	36
NG4-2000-1	R_h (nm)-2 mM SDS	22.5	21	19	17
NG5-5000-0.05	R_h (nm)-pure water	20	23	27	26
NG5-5000-0.05	R_h (nm)-2 mM SDS	22	20	16	14
NG6-5000-0.5	R_h (nm)-pure water	23	33	36	35
NG6-5000-0.5	R_h (nm)-2 mM SDS	24	22	18.5	17
NG7-5000-1	R_h (nm)-pure water	30	34	36	33
NG7-5000-1	R_h (nm)-2 mM SDS	35	33	30	24
NG8-13000-0.05	R_h (nm)-pure water	23	24	24	22
NG8-13000-0.05	R_h (nm)-2 mM SDS	28	18	18.5	17.5

Appendix IV: Asymmetric Flow Field–Flow Fractionation (AF4) measurements

To determine the polydispersity of the nanogels, AF4 measurements were performed as a qualitative method, giving a comparison between widths of distribution of different nanogels. The width of distribution from AF4 was compared with β values from DLS. Figure shows the intensity of detected light scattering signal at angle of 90° vs. elution time for three different nanogels (NG1, NG2-2000-0.05 and NG3-2000-0.5). The fractogram indicates that, as the surface concentration of PEG layer increases, size distribution of nanogels broadens. This difference in polydispersity is more pronounced in AF4 compared to β from DLS result.

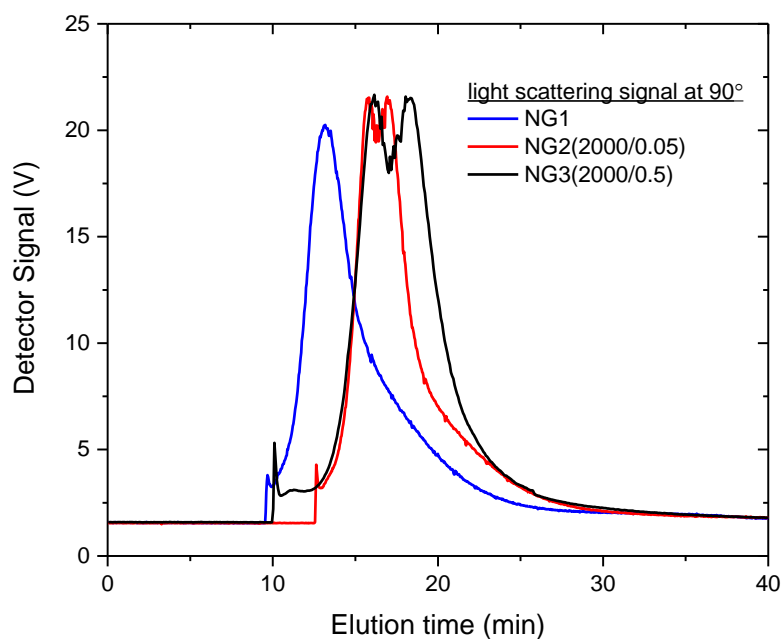


Figure 6-1: AF4 fractogram of intensity of scattered light at 90° angle vs. elution time for three samples (NG1, NG2-2000-0.05 and NG3-2000-0.5 with different PEG surface concentration. NG1 has no PEG layer and other sample have 0.05 and 0.5 mole % of PEG-2000, respectively.

The fractogram for NG7-5000-1 (sample with highest PEG content) is illustrated in Figure . The fractogram shows a very broad size distribution for this sample and the main peak is almost split in two peaks. The DLS results also indicated that NG7-5000-1 has a broad size distribution ($\beta = 0.81$) which is in good agreement with what was found by AF4 measurements for this sample.

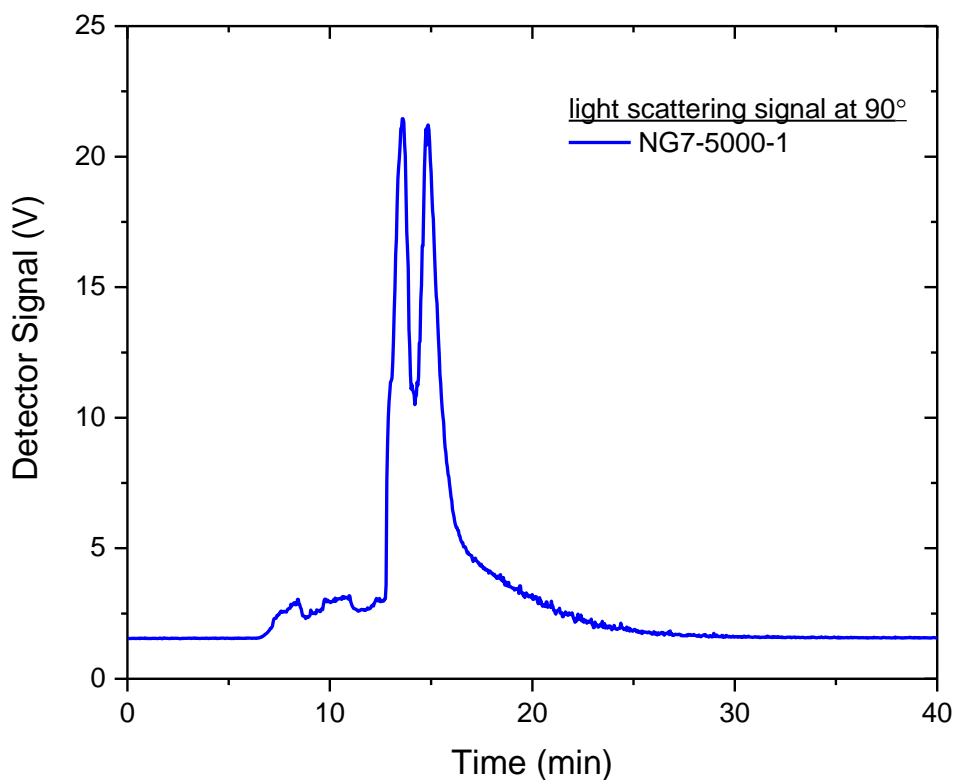


Figure 6-2: AF4 fractogram of intensity of scattered light at 90° angle vs. elution time for NG7-5000-1 with 1 mole % surface concentration of PEG-5000.